Evaluation of the micro liquid|liquid interface towards electroanalytical detection of Fe^{2+} and trace metal ions in terrestrial and seawater

by

Qi Jiang

A thesis submitted to the School of Graduate Studies in partial fulfillment of the requirements for the degree of

Master of Science

Department of Chemistry

Memorial University of Newfoundland and Labrador

St. John's, Newfoundland

August 2021

Abstract

As the primary production of phytoplankton is the foundation of the global carbon cycle, monitoring the spatiotemporal concentration of iron, which is a key micronutrient often limiting the growth of phytoplankton in the ocean, has been a focus in oceanic and terrestrial waters for several decades. Herein, we propose to evaluate a novel method of iron detection at a micro interface between water|1,2-dichloroethane (w|DCE) and water|ionic liquid (w|IL). Ligand assisted charge transfer of Fe^{2+} was monitored electrochemically using cyclic and differential pulse voltammetry (CV and DPV). Chapter 1 introduces some techniques used for detection of iron in the seawater and contemporary analytical methods in the field, as well as fundamental concepts of electrochemistry at the interface between two immiscible electrolyte solutions (ITIES), so-called liquid|liquid electrochemistry. Chapter 2 describes the main body of work in which four ligands were investigated toward facilitated Fe^{2+} transfer, including 1,10-phenathroline (phen), 1-nitroso-2-naphthol (N2N), 2-(2-thiazolylazo)-p-cresol (TAC), and salicylaldoxime (SAL). The overall complexation or binding constant for each ion was determined and compared versus Fe^{2+} coordination at the w|DCE micro-interface. Three Fe^{2+}:phen, metal:ligand, stoichiometries were observed; however, only a single stoichiometry was recorded in the case of the other ligands. Chapter 3 describes a preliminary investigation of facilitated Fe^{2+} transfer reactions using phen at a water|ionic liquid (w|IL) interface, while Chapter 4 provides some overall conclusions and perspectives as to the direction of the field moving forward.

Acknowledgements

I would first like to express my sincere gratitude to my supervisor Dr. Talia Jane Stockmann for her continuous support throughout my program and her patient suggestion to my thesis. Thanks to her instruction, I have learned a great deal here.

Then, both during my experiments and in life, my lab mates: Reza, Siamak, Ahbi, and Nazanin, who have given me great help when I was stuck on problems.

At last, I appreciate my parents supporting me firmly all the time and give me spiritual and material support so that I can achieve my personal life goals.

Contents

List of Figures

List of Tables

List of Abbreviations

AAS: Atomic Absorption Spectroscopy

ACT: Aqueous Complexation followed by Transfer

CV: Cyclic Voltammogram or Cyclic Voltammetry

DCE: 1,2-dichloroethane

DPV: Differential Pulse Voltammetry

EC′: Electrochemical-Catalytic Mechanism

FIT: Facilitated Ion Transfer

HMDE: Hanging Mercury Drop Electrode

HNLC: High-nutrient and Low Chlorophyll

IL: Ionic Liquid

ITIES: Immiscible Interface between Two Immiscible Electrolyte Solutions

LOD: Limit of Detection

N2N: 1-nitroso-2-naphthol

$P_{8888}TB$: Tetraoctylphosphonium tetrakis(pentafluorophenyl)borate

phen: 1,10-phenathroline

PPW: Polarizable Potential Window

TAC: 2-(2-thiazolylazo)-p-cresol

TB: $B(C_6F_5)_4^-$ or tetrakis(pentafluorophenyl)borate

TIC: Transfer by Interfacial Complexation

TID: Transfer by Interfacial Decomplexation

TMACl: Tetramethylammonium chloride

TOC: Transfer followed by Organic Phase Complexation

SAL: Salicylaldoxime

List of Symbols

A: ampere

α (subscript): refers generally to a phase

a_i: the activity of the ion

β: overall complexation constant

o: (superscript): refers being at thermodynamic standard state.

$D_{i,\alpha}$: diffusion coefficient of ion, i in phase α

$\Delta_o^w\phi$: Galvani potential difference across a water (w)|oil (o) interface

$\Delta_o^w\phi_{1/2}$: half-wave potential

$\Delta_o^w\phi_{i^z}^{o'}$: formal ion transfer potential of ion, i with charge z

$\Delta_o^w\phi_{1/2}$: the half-wave potential

E: potential

η: viscosity

F: Faraday's constant

I: current

L: liter

L: ligand

M: refers generally to a metal ion

ML_n^z : the metal ion and ligand complex with a stoichiometry of n and charge z

min: minute

mM: millimolar

$\tilde{\mu}$: electrochemical potential

μ: chemical potential

μm: micrometer

nA: nano ampere

n: ligand stoichiometry

v: scan rate

ϕ_{α} : potential in phase α

R: the gas constant

s: second

T: temperature

V: voltage (volts)

w|o: water|oil

w|IL: water|ionic liquid

z_i: charge of ion

$\xi = \sqrt{D_{i,\mathrm{IL}} / D_{i,w}}$

Chapter 1

Introduction

1.1 Iron in Ecosystems

The primary production of phytoplankton plays an important role in transferring carbon from the atmosphere to the marine system through a process called the biological carbon pump.[1] However, iron is a necessary element for nitrogenase, the primary enzyme responsible for nitrogen fixation within phytoplankton,[2] making the concentration of iron restrict the growth of phytoplankton in the ocean. Since Fe^{2+} is easily oxidized to Fe^{3+}, which has low solubility, iron usually persists as colloids, nanoparticles, or organically binding with ligands[3] or as carbonates or oxides.[2] Iron in the open ocean mainly comes from the atmosphere in the form of dust blown from continental sources; however, continental shelf sediments, hydrothermal vents, rivers, and melting glaciers in polar regions also contribute.[2] It is removed by biological absorption, scavenging, precipitation, and sedimentation.[2] To survive iron stress in so-called high-nutrient, low chlorophyll (HNLC) zones where iron concentrations are low, phytoplankton has evolved some architectural changes within their photosynthetic membranes with improved iron-economy.[4] Given the primary production of phytoplankton as the foundation of the global carbon circle, it is meaningful to understand the spatial and temporal iron concentration distributions in the coastal and open ocean. In this section, common analytical methods of iron characterization in environmental samples are reviewed and the fundamental electrochemistry at liquid|liquid interfaces is introduced.

1.2 Analytical Methods

1.2.1 Atomic Absorption Spectroscopy

Atomic absorption spectroscopy (AAS) is one of the most widely used analytical methods for determining iron content in seawater with iron concentrations in the sub-nanomolar range.[5] AAS was developed by Robert Wilhelm Bunsen and Gustav Robert Kirchhoff in the middle of the 19th century[6] and it has been subject to much modification and improvement since then, such that it is widely used to detect iron in seawater as a mature technique. Kojuncuv *et al*.[7] proposed a method by using cobalt(III) hexamethylenedithiocarbamate, $Co(HMDTC)_3$, as a flotation collector to separate the heavy metal ions, such as Cd, Cu, Pb, Fe, in seawater before their analysis by AAS. The limits of detection of those metal ions were obtained as 0.010 µg/L for Cd, 0.034 µg/L for Cu, 0.305 µg/L for Ni, 0.290 µg/L for Pb, 0.032 µg/L for Tl, 0.890 µg/L for Fe, and 0.994 mg/L for Zn. Additionally, the assessment of heavy metals in the sediments of Ondo coastal marine area were studied by Tunde *et al*.[8] with AAS. They used sediment enrichment factor (K_{sef}), contamination factor (C_f^i), and modified degree of contamination (mC_d), sediment quality guidelines (SQG), sediment toxicity degree (ST_d) and toxicity load index (TLI) to evaluate the degree of pollution.

1.2.2 Spectrophotometry Methods

Spectrophotometry is another efficient spectroscopic technique involving coloured iron-ligands complexes with high molar absorptivity,[9] which has been widely used for detection of iron in seawater because of its diversity and flexibility. 1,10-phenanthroline was one of the earliest selective iron ligands employed.[9] In 1957, Armstrong[10] recognized that much of iron in seawater

is sequestered in particulate form; however, they were investigating the possible spectrophotometric interference of iron quantification from fluoride ions, which are present at appreciable amounts in seawater. Samadi-Maybodi *et al*.[11] created an Fe^{2+} selective sol-gel based spectrophotometric platform incorporating the ligand 2,4,6-tri(2-pyridyl)-s-triazine, which is often employed for iron determination in seawater,[9] with a limit of detection of 1.68 ng/mL. Increasingly more iron-selective ligands are being sought in order to overcome matrix effects such as competing metal ions.

With this in mind, a sensitive spectrophotometry method was proposed by Asan, A *et al*.[12] in which 2', 3, 4', 5, 7-pentahydroxyflavone (morin) which reacted with Fe^{2+} selectively in a slightly acid solution generating a Fe^{2+}-morin ligand which possesses a strong absorption band at 415 nm; a limit of detection of 3 μg/L, the determination of Fe^{2+}, and total iron in water samples was obtained. Miranda *et al*.,[13] employing solid-phase spectrophotometry coupled with a hexadentate 3,4–hydroxypyridinone ligand, were able to demonstrate high specificity for iron detection over interfering metal ions like Mg^{2+} and Pb^{2+}. More recently, Huang *et al*.[14] developed a flow injection (FI) method based on the catalytic, chemiluminescence (CL) of iron bound to N,N-dimethyl-p-phenylenediamine dihydrochloride (DPD) for the measurement of Fe^{2+} and Fe^{3+} in seawater samples from the South China Sea. They were able to achieve a minimum detection limit of 43 pmol/L without a preconcentration step which was equivalent to other contemporary methods that employ one, by combining the FI-CL method onto a nitrilotriacetic acid (NTA) Superflow resin coupled with a long pathlength waveguide capillary cell (LWCC). In this way, they were able to evidence sub-nanomolar detection levels, which is necessary as these are the typical concentrations of iron in the open ocean.

1.2.3 Electrochemical Methods

Electrochemical methods have also been widely employed in the detection of iron in seawater and are valuable owing to their ability to differentiate between Fe^{2+} and Fe^{3+} redox species.[9,14,15] Redox speciation of iron in the open ocean is significant as Fe^{2+} is more bioavailable/soluble, however, Fe^{3+} is more thermodynamically favored and thus microorganisms have developed different strategies for coping with low iron concentrations, which, as mentioned above, are typically in the sub-nanomolar range.

1.2.3.1 HMDE

A critical electrochemical instrument was invented by J. Heyrovsky *et al*.[16] in 1922 called the dropping mercury electrode (DME) as it produces a sequence of droplets of mercury of controlled size growth at the end of a capillary which is immersed in an aqueous solution while the potential across the Hg-droplet|water interface is controlled using a potentiostat connected in a three electrode configuration. In this case, Hg is connected to the working electrode lead, while a counter and reference electrode are immersed in the aqueous phase at a distance from the Hg droplet. Potential controlled experiments of this type are referred to as polarography. However, DME has a constantly changing area, which makes the treatment of diffusion difficult to manage, which is further complicated by a continuous double-layer background charging current.[16] Additionally, Hg forms amalgams with many different metals resulting in loss of metal analytes to the Hg phase and complicating their analytical quantification. However, this is only a complication on longer time scales; for instance, in the pool of liquid Hg that accumulates at the bottom of flask in which the DME operates. Therefore, to avoid these drawbacks, the hanging mercury drop electrode (HMDE) was developed. HMDE has a static surface area with a well-established geometry|surface area at the end of a capillary (see Figure 1.1).

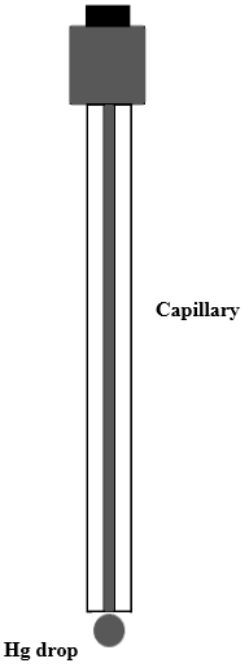

Figure 1.1: Structure of hanging mercury drop electrode (HMDE)

Many studies have employed HMDE coupled with cathodic stripping voltammetry (CSV) and ligands which adsorb an Fe-complex at the Hg surface[17,18] or using an oxidizing agent added to the bulk, aqueous solution.[19] The latter takes advantage of the EC′ (E = electrochemical; C′ = catalytic) mechanism in which Fe^{3+} is reduced at the HMDE and then re-oxidized by the oxidizing agent in solution generating a catalytic current (see Figure 1.2). For example, Obata et al.[20] employed BO_3^- as the oxidizer to reach sub-nanomolar detection levels.

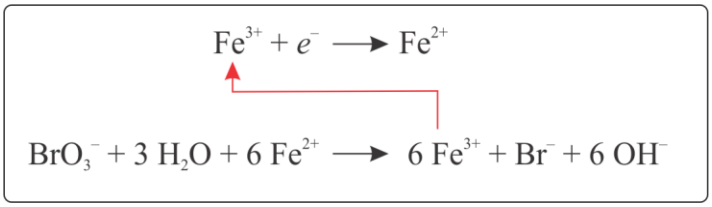

Fig. 1.2: Electrochemical-Catalytic (EC′) mechanism exploited by Obata *et al.*[20] for enhanced detection of Fe^{3+} in seawater at an HDME.

Van den Berg's group [18] found that by adding EDTA to the solution one can reduce the interference of copper or lead; however, naturally occurring organic surfactants need to be removed by UV-irradiation of the sample. Genovese et al [21] applied the adsorption CSV method, with 1-nitroso-2-naphthol (N2N) as the ligand, to detect dissolved iron-organic ligand speciation parameters in Antarctic sea-ice. Their results showed that Fe-binding ligands in pack ice were not Fe-saturated and that these so-called 'Fe-free ligands' could be a contributor to aiding in the solubility/bioavailability of dissolved-Fe in the open ocean once they are released from the ice; moreover, that the loss of sea-ice would result in a loss of free ligands and in turn, the amount of bioavailable dissolved-Fe.

1.2.3.2 Modified Electrodes

The surface of a modified electrode can be directionally modified to meet the requirement of targeted properties, more effective in detection of iron. Indeed, much research has been finished with modified electrodes. Li *et al*.[22] used Nafion to stabilize ionic liquid-reduced graphene oxide (IL-rGO) supported gold nanodendrites (AuNDs) on a glassy carbon electrode in order to provide larger specific surface area to promote the Fe^{3+} reduction process. With an advantageous anti-interference property, a limit of detection of 35 nM of Fe^{3+} was reached, performing well in the detection of iron in coastal areas. Ma *et al*.[23] attached the cation of methylene blue (MB) and $PtCl_6^{2-}$ to a graphene oxide (GO) surface and deposited the assembly onto a GCE electrode; afterwards, $LiBH_4$ was used to reduce each component such that the final electrode composite consisted of reduced graphene oxide/leucomethylene blue/platinum nanoparticles (rGO/LMB/PtNPs/GCE). Given a linear range of 0.01 to 2 μM and a detection limit of 3 nM, this modified electrode was applied to the detection of iron in seawater.

1.2.3.3 Alloy Electrodes

Compared to HDMEs, alloy electrodes are more environmentally friendly and less technically challenging to operate. Indeed, more studies are turning to this strategy in this emerging field of biogeochemical analysis. For example, Mikkelsen *et al*.[24] employed a rotating Ag/Hg-alloy (like dental amalgam) disk electrode to detect dissolved iron in seawater by differential pulse anodic stripping voltammetry (DPASV) with a limit of detection (LOD) of 0.3 nM upon application of a 900 s plating time; this necessitates the deposition of elemental iron (*i.e.*, $Fe^{2+} + 2e^{-} \rightarrow Fe^{0}$). Critically, using this method they were able to show that after addition of a ligand like EDTA, the iron peak disappeared; therefore, the silver-alloy electrode could be used to differentiate between dissolved or weakly complexed iron, which the group categorized as labile, and that of strongly complexed iron.[25] Similarly, Lin *et al*.[25] fabricated a tin-bismuth alloy electrode (SnBiE) that was able to obtain a LOD of 0.2 nM for dissolved iron in coastal regions after only a 60 s accumulation time. As mentioned recently by Zhang *et al*.,[26] alloy electrodes employing Bi, Sb, and Sn are advantageous as they are more environmentally friendly and often have higher sensitivity towards the detection of heavy metal ions, including iron. Moreover, they can be constructed at a lower cost, require a smaller lab footprint, and are more technically convenient to use; this makes them ideal as well for ship-board measurements or as continuous monitoring sensors deployed in coastal waters or the open ocean. Alloy electrodes also provide a mechanism for total organic ligand quantifications. However, the determination of thermodynamic binding coefficients, a critical parameter for many electrochemical, adsorptive techniques, is often an indirect measurement and thus herein, we propose to use electrochemistry at the interface between two electrolyte solutions (ITIES) which has been well-developed for direct determination of metal ion complexation thermodynamics.

1.3 Liquid|Liquid Electrochemistry

Electrochemistry at an ITIES has several advantages: it is molecularly smooth, reproducible, and does not require polishing or surface characterization like solid electrodes.[27] Current across the ITIES is a function of charge transfer $\left(i = \frac{dQ}{dt} \right)$ like that at a solid/solution interface; however, at a liquid|liquid interface charge transfer extends to the flux of charged species crossing the interface, which is commonly called simple and facilitated ion transfer. In this way, the ITIES formed between water|oil (w|o) is biomimetic, *i.e.*, it can be used as a first approximation for charge transfer across cellular membranes of living cells. Of analytical importance is that all of the voltammetric and pulse profile theoretical treatments (*e.g.*, the Randles-Sevčik equation) can be transposed from the solid|solution interface to the liquid|liquid one.

1.3.1 Simple Ion Transfer

Simple ion transfer refers to the transfer of a charged species, such as an ion, i with charge z_i, from the aqueous (w) to organic (o) phase, or vice versa [28], and can be described by equation 1.1.[29]

$$i_w^{z_i} \rightleftharpoons i_o^{z_i} \tag{1.1}$$

The electrochemical potential of i, defined as $\tilde{\mu}_i$, can be described in either phase as,

$$\tilde{\mu}_{\alpha,i} = \mu_{\alpha,i}^{o} + RT \ln\left(a_{\alpha,i}\right) + z_i F \phi_\alpha \tag{1.2}$$

Where $\mu_{\alpha,i}^{o}$ and $a_{\alpha,i}$, are respectively the standard chemical potential and activity of ion i in phase α, while ϕ_α is the Galvani potential in phase α. Meanwhile, R, F, and T are the gas constant,

Faraday constant, and temperature in Kelvin, respectively. At an immiscible liquid|liquid interface between water|oil (w|o) at equilibrium, equation 1.2 can be expanded to obtain,

$$\mu^{o}_{w,i} + RT\ln\left(a_{w,i}\right) + z_i F\phi_w = \mu^{o}_{o,i} + RT\ln\left(a_{o,i}\right) + z_i F\phi_o \tag{1.3}$$

Indeed, the interfacial Galvani potential difference of *i*, $\Delta^{w}_{o}\phi$, can be obtained through rearrangement of 1.3 such that,

$$\Delta^{w}_{o}\phi = \phi_w - \phi_o = \frac{\mu^{o}_{w,i} - \mu^{o}_{o,i}}{z_i F} + RT\ln\left(\frac{a_{w,i}}{a_{o,i}}\right) \tag{1.4}$$

Since the Gibbs energy, $\Delta G^{o}_{i,tr\,w\to o} = \mu^{o}_{w,i} - \mu^{o}_{o,i}$, which is related to the standard ion transfer potential *via*, $\Delta^{w}_{o}\phi^{o}_{i,tr\,w\to o} = \frac{\Delta G^{o}_{i,tr\,w\to o}}{z_i F}$. Thus, the Nernst equation for a simple ion transfer process is:

$$\Delta^{w}_{o}\phi = \Delta^{w}_{o}\phi^{o}_{i,tr\,w\to o} + \frac{RT}{z_i F}\ln\left(\frac{a_{w,i}}{a_{o,i}}\right) \tag{1.5}$$

Throughout this work a miniaturized liquid|liquid interface was employed similar to that depicted in Figure 1.3. Two electrodes, one immersed in either phase, were used to modify the Galvani potential difference across the interface. The pipette holder with an integrated electrode was connected to the working electrode lead of a potentiostat, while a counter electrode was placed in the external phase. The pipette tip containing the aqueous phase was immersed into the organic solution and the ITIES was maintained at the tip.

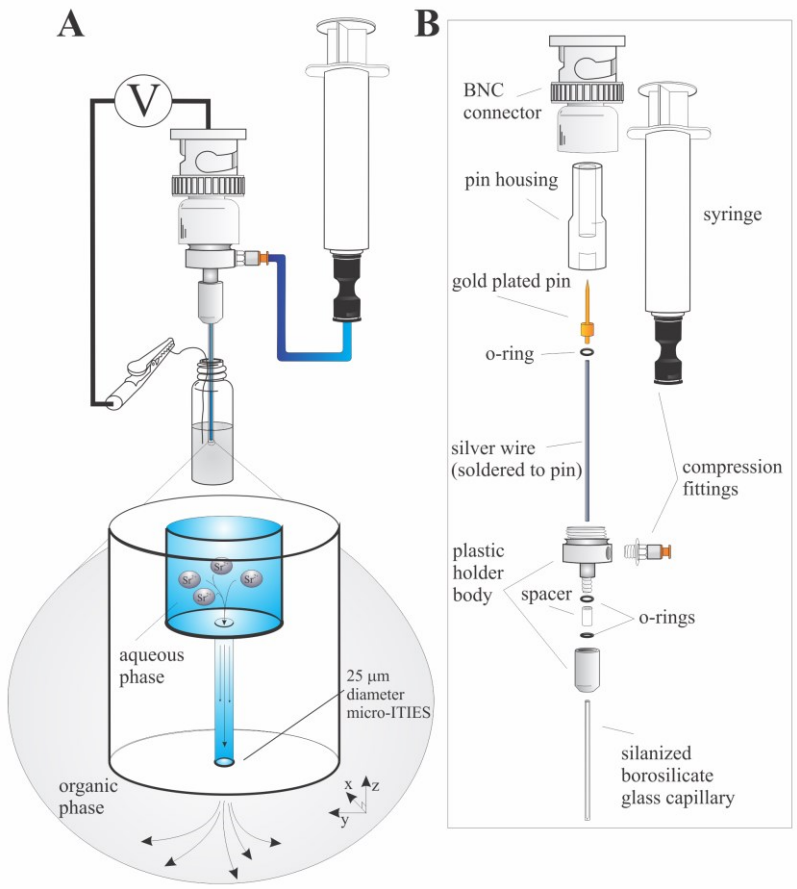

Figure 1.3: (A) Micropipette holder with integrated working electrode connected to a BNC connector with expanded view of the ITIES at the pipette tip. (B) Exploded view of the holder; reprinted from.[30]

1.3.2 Facilitated Ion Transfer

Facilitated ion transfer is a mechanism whereby a ligand (L) mediates ion transfer across the ITIES[31] and can be described generally through equation 1.6,

$$i_w^{z_i} + nL_o \rightleftharpoons iL_{n,o}^{z_i} \tag{1.6}$$

where n is the ligand's stoichiometric coefficient.

According to Reymond's[32] work, there are 3 dominant mechanisms for a hydrophilic ion positioned in the aqueous phase combining with a hydrophobic ligand dissolved in the organic phase: (1) transfer by interfacial complexation (TIC)/decomplexation (TID); (2) transfer followed by organic phase complexation (TOC); and (3) aqueous complexation followed by transfer (ACT). See Figure 1.4 for a diagram of each of these mechanisms.

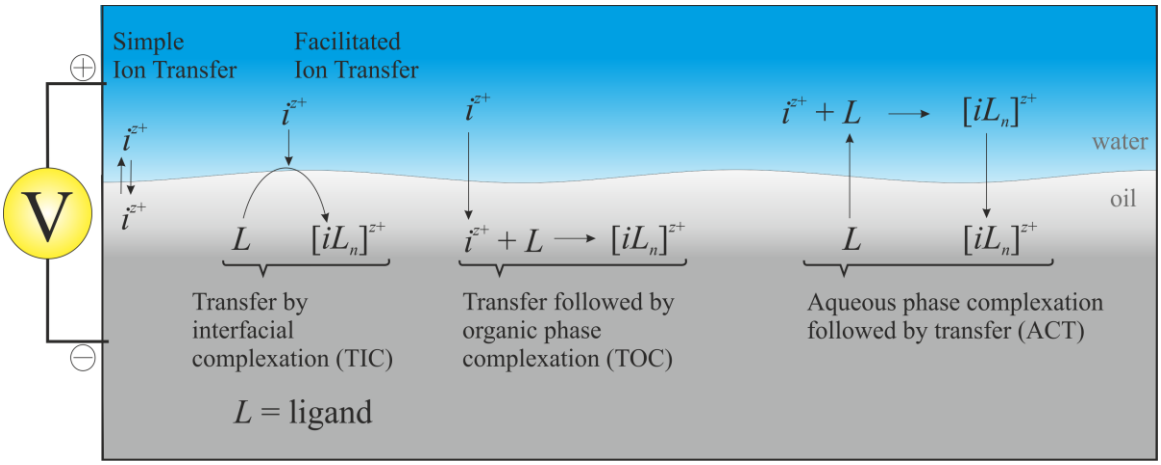

Figure 1.4: Expressions for the three dominant facilitated ion transfer mechanisms.

In the case in which the ligand is in excess concentration with respect to the metal ion and the ligand is hydrophobic, such that the TIC mechanism is preferred, Reymond *et al.*[33] showed that a linear relationship can be derived, [33]

$$-\frac{zF}{RT}\left(\Delta_o^w\phi_{1/2,iL_n^{z_i}}-\Delta_o^w\phi_{i^{z_i}}^{o'}\right)=n\ln\left(c_L^*\right)+\ln\left(\beta\right) \qquad (1.7)$$

Where $\Delta_o^w\phi_{1/2,iL_n^z}^{o'}$ is the half-wave transfer potential of the metal ion–ligand complex which varies depending on the initial ligand concentration, $c_{L,\text{initial}}$. $\Delta_o^w\phi_{i^z}^{o'}$ is the formal ion transfer potential of the free metal ion. Critically, in equation 1.7, the stoichiometry can be obtained from the slope, while the overall complexation constant (β) can be calculated from the y-intercept.

1.4 Scope of This Thesis

The goal of this work was to evaluate the feasibility of the liquid|liquid interface as an electroanalytical platform for the quantification of total dissolved iron in sea, coastal, and estuary waters. Unfortunately, owing to time constraints and delays due to Covid-19 lockdown, environmental samples were never properly tested, and a routine methodology is still under development.

In chapter 2, experiments at a w|DCE micro-interface, with $P_{8888}TB$ (tetraoctylphosphonium tetrakis(pentafluorophenyl)borate) as a supporting electrolyte in the organic phase, successfully evaluated the relationship between the Fe^{2+} dissolved in the aqueous phase and 4 hydrophobic ligands, including 1,10-phenathroline (phen), 1-nitroso-2-naphthol (N2N), 2-(2-thiazolylazo)-p-cresol (TAC), and salicylaldoxime (SAL). This work has been published in *ChemElectroChem.*[34]

In chapter 3, the investigations were expanded to focus on a water|ionic liquid (w|IL) interface in which $P_{8888}TB$ was used a model IL operating at ~60 °C. This work is still in a preliminary state; however, promising results have been obtained for phen.

Finally, chapter 4 will provide a perspective on the field and where research is headed.

1.5 References

[1] R. F. Strzepek, P. W. Boyd, W. G. Sunda, *Proc. Natl. Acad. Sci. U. S. A.* **2019**, *116*, 4388-4393

[2] P. J. Worsfold, M. C. Lohan, S. J. Ussher, A. R. Bowie, *Mar. Chem.* **2014**, *166*, 25-35.

[3] P. W. Boyd; M. J. Ellwood, *Nat. Geosci*. **2010**, *3*, 675-682.

[4] M. J. Behrenfeld, and A. J. Milligan, *Ann. Rev. Mar. Sci*., **2013**, 5 , 217–246.

[5] W. M. Landing, K. W. Bruland, *Geochim. Cosmochim. Acta* **1987**, *51*, 29-43.

[6] B. Welz, M. Sperling (1999), Atomic Absorption Spectrometry, Wiley-VCH, Weinheim, Germany, ISBN 3-527-28571-7.

[7] Ý. Kojuncu, J. M. Bundalevska, Ü. Ay , K. Čundeva, T. Stafilov, and G. Akçin, *Sep. Sci. Technol*., **2004**, *39,* 2751–2765.

[8] O. L. Tunde, and A. P. Oluwagbenga. J. *Afr. Earth Sci*. **2020**, *170, 103903.*

[9] M. Lin, X. Hu, D. Pan, and H. Han. *Talanta*, **2018**, *188*, 135–144.

[10] F. A. J. Armstrong, *J. Mar. Biol. Assoc. U. K*., **1957**, *36*, 509–517.

[11] A. Samadi-Maybodi, V. Rezaei, S. Rastegarzadeh, Spectrochimica Acta Part A: Molecular and Biomolecular Spectroscopy. **2015,** *136*, 832-7

[12] A. Asan, R. Aydin, D.K. Semiz, V. Erci, and I. Isildak. *Environ. Monit. Assess.*, **2013**, *185*, 2115–2121.

[13] J. L. A. Miranda, R.B.R. Mesquita, A. Nunes, M. Rangel, and A.O.S.S. Rangel, *Talanta*, **2019**, *191*, 409–414.

[14] Y. Huang, J. Xu, L. Chen, D. Yuan, S. Feng, and Y. Cai, *Microchem. J*., **2021**, *162*, 105840.

[15] Á. Molina, J.M. Olmos, and E. Laborda, *Sens. Actuators B Chem.*, **2017**, *253*, 326–334.

[16] I. M. Kolthoff, J.J. Lingane, *Chem. Rev.* **1939**, *24*, 1-94

[17] M. Gledhill, C.M.G. van den Berg, *Mar. Chem*. **1995**, *50*, 51-61

[18] C.M.G. van den Berg, and Z.Q. Huang. *J. Electroanal. Chem. Interfacial Electrochem.*, **1984**, *177*, 269–280

[19] A. Bobrowski, J. Zarębski, Electroanalysis **2000**, *12*, 1177-86

[20] H. Obata, C. M. G. van den Berg, *Anal. Chem*. **2001**, *73*, 2522-2528

[21] C. Genovese, M. Grotti, J. Pittaluga, F. Ardini, J. Janssens, K. Wuttig, S. Moreau, D. Lannuzel, *Mar. Chem.* **2018**, *203*, 28-37

[22] F. Li, D. Pan, M. Lin, H. Han, X. Hu, and Q. Kang, *Electrochim. Acta*, **2015**, *176*, 548–554.

[23] S. Ma, D. Pan, H. Wei, N. Wang, F. Pan, , and Q. Kang. *Microchem. J.*, **2019**, *151*, 104210.

[24] Ø. Mikkelsen, C.M.G. van den Berg, and K.H. Schrøder. *Electroanalysis*, **2006**, *18* , 35–43

[25] M. Lin, D. Pan, X. Hu, F. Li, and H. Han. *Anal. Methods*, **2015**, *7* , 5169–5174.

[26] X. Zhang, K. Qu, and D. Li. *Int. J. Electrochem. Sci.* **2015**, *10*, 8497–8512.

[27] M. D. Scanlon, E. Smirnov, T. J. Stockmann, P. Peljo, *Chem. Rev*. **2018**, *118*, 3722-3751

[28] L. J. Sanchez Vallejo, J. M. Ovejero, R. A. Fernández, S. A. Dassie, *Int. J. Electrochem*. **2012**, 1–34

[29] S. Liu, Q. Li, Y. Shao, *Chem. Soc. Rev. 40*, **2011**, 2236-53

[30] T. J. Stockmann, A.-M. Montgomery, Z. Ding, *Can. J. Chem*. **2012**, *90*, 836-42

[31] P. Peljo, H. H. Girault, in Encyclopedia of Analytical Chemistry, John Wiley & Sons, Ltd, **2012**.

[32] F. Reymond, G. Lagger, P.-A. Carrupt, and H.H. Girault. *J. Electroanal. Chem.*, **1998**, *451*, 59–76.

[33] T. J. Stockmann, Y. Lu, J. Zhang, H.H. Girault, Z. Ding, *Chem. Eur. J.*, **2011**, *17*, 13206-13216

[34] Q. Jiang, H.E. Reader, and T.J. Stockmann, *ChemElectroChem*, **2021**, *8*, 1580–1587.

Chapter 2

Electrochemical Characterization of $Fe^{2}+$ Complexation at an Aqueous|DCE Interface

2.1 Statement of Co-Authorship

This chapter has been published under the above title in *ChemElectroChem* **2021**, *8*, 1580–7.

Authors: Qi Jiang, Dr. Heather E. Reader, Dr. T. Jane Stockmann

This article was a collaboration between the Stockmann and Reader labs. Q. Jiang is the first author as he performed the 95% of the experimental work and analyzed the data. TJS designed the experiments, wrote the first draft of the manuscript, performed data analysis, and finally edited as well as finalized the manuscript. HER helped design the experiment, write the first draft, and edit as well as finalized the manuscript.

2.2 Abstract

Phytoplankton growth in the open ocean is critical to carbon fixation and often limited by low iron concentrations. Owing to its low solubility, phytoplankton employ ligands for iron uptake; therefore, ligand binding characterization is important. Herein, a micro immiscible liquid|liquid interface was employed with four ligands through an electrochemically induced facilitated ion-transfer process. Ligands 1,10-phenathroline (phen), 1-nitroso-2-naphthol (N2N), 2-(2-

thiazolylazo)-p-cresol (TAC), and salicylaldoxime (SAL), were tested using established facilitated ion-transfer thermodynamics combined with differential pulse voltammetry. Three metal ion/ligand binding stoichiometries were observed for Fe^{2+}:phen, whereas only one was observed with Fe^{2+} with SAL, N2N, and TAC. Overall binding constants were calculated such that binding strengths can be ranked highest to lowest as phen>N2N>TAC>SAL. Additionally, the formal ion transfer for Fe^{2+} (0.66 V) for an aqueous|1,2-dichloroethane interface was also determined.

2.3 Table of Contents Graphic:

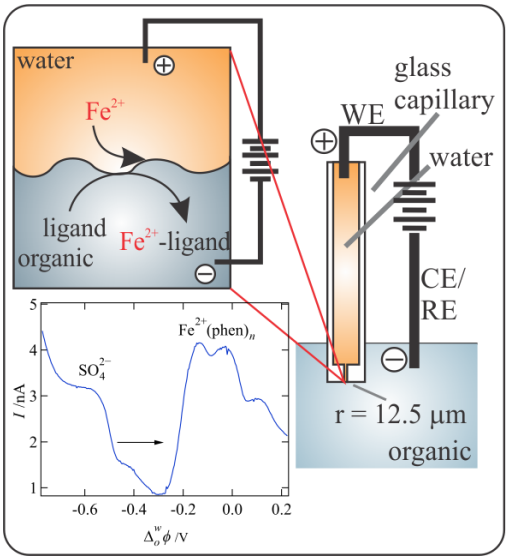

2.4 Introduction

Phytoplankton growth and productivity forms the foundation of ecology within the world's oceans.[1] 50% of all photosynthesis worldwide is performed in the oceans and oceanic processes are dominated by phytoplankton.[1-2] However, phytoplankton growth is limited in vast areas of

the ocean by the lack of biologically available nitrogen (so-called "High Nutrient – Low Chlorophyll" zones). Nitrogenase, the primary enzyme responsible for fixing nitrogen, requires iron and it is the insolubility of iron that limits growth in many areas of the open ocean.[3] Phytoplankton have evolved to take advantage of iron complexation with organic ligands that maintain dissolved iron concentrations in the surface ocean, for example, the production of siderophores by marine microorganisms. Given that phytoplankton are key to carbon fixation and iron often limits their growth,[4] monitoring the spatial and temporal iron concentration distributions in the coastal and open ocean is of critical importance to understanding marine productivity as well as the global carbon cycle.

Several analytical methods have been developed for laboratory and ship-board[5] testing of seawater samples whose iron concentrations are in the sub-nanomolar range[6] including, atomic absorption spectroscopy (AAS),[7] spectrophotometry,[8] chemiluminescence,[9] and voltammetry.[6, 10] Early methods employed double extraction or solvent extraction, pre-concentration steps to achieve ~50 pmol/L detection limits. For example, Bruland *et al.*[7a] used the ligands ammonium 1-pyrrolidinedithiocarbamate and diethylammonium diethyldithiocarbamate in a double extraction into chloroform, then back-extracted the iron into an aqueous solution using nitric acid; the aqueous phase was subsequently analyzed *via* AAS. Similarly, ligands highly selective for iron have been used in spectrophotometric methods such as 1,10-phenanthroline[8] (phen) with detection limits in the same region. Ligand usage in spectrophotometric methods may influence the redox speciation of iron between Fe^{2+} and Fe^{3+}.[11]

Since the 1980's, electrochemical methods of detection have relied on the hanging drop mercury electrode (HDME) often coupled with adsorptive cathodic stripping voltammetry to

achieve ultra-trace detection of iron in sea and fresh waters. [5a, 10d, 10k, 10l, 12] For example, van den Berg's group has used catechol,[10l] 1-nitroso-2-naphthol (N2N),[10h-k] as well as 2,3-dihydroxynaphthalene (DHN),[5b] as absorptive and competitive ligands for iron detection and reported sub-nanomolar limits of detection (LOD). In 2001, Obata *et al*.[5a] were able to catalytically enhance the reduction current of the adsorbed Fe^{3+}-DHN using bromate added to the aqueous phase through an EC′ (E = electrochemical step; C′ = catalytic chemical step) mechanism[13] in which electrode generated Fe^{2+} is re-oxidized by BrO_3^- in solution. Afterwards, Capara *et al*.[10p] were able to achieve similar sensitivities, however, using dissolved O_2 as the oxidizer. These ligands compete with naturally occurring organic ligands as well as the formation of inorganic iron species such as colloids and Fe nanoparticles. Natural ligands often take the form of exopolymeric substances thought to be generated by bacteria and algae which protect these organisms from the high salinity/ionic strength and low temperatures of seawater in areas like the North Atlantic, Arctic, and Antarctic regions.[14] More recently it has been recognized that humic substances[10a, 15] released from terrestrial sources are a rich source of iron binding ligands. Indeed, Genovese *et al*.[10n] through a similar technique investigated iron speciation within Antarctic pack/fast ice utilizing N2N as the competitive/absorptive ligand. One advantage of voltammetric methods is they can discriminate between iron redox states[6b, 10d] through either direct Fe^{3+} reduction or cathodic stripping techniques employing iron-specific complexing agents. [5, 10a, 10b, 10d-r]

The above-mentioned electrochemical investigations all employed HDMEs which have inherent technical challenges and toxicity; recent studies have turned to modified electrodes or novel electrode materials. Lin *et al*. employed a tin-bismuth alloy electrode (SnBiE) in combination with the ligand 1-(2-pyridylazo)-2-naphthol and cathodic stripping voltammetry to

achieve a LOD of 0.2 nM. Meanwhile, Liu *et al*.[16] modified the surface of a glassy-carbon electrode with Au nanoparticles whose surface was functionalized using N-carboxy-L-cysteine for Fe^{3+} detection. The high affinity of the sulfur moiety of the cysteine group towards Au was exploited as the means to bind to the nanoparticle surface, while the carboxylic acid group bound and concentrated dissolved Fe^{3+} at the nanoparticle/electrode surface.[16] Combined with their ultra-trace level (sub-nanomolar) detection, small laboratory footprint, cost, and relative ease of use, electrochemical methods are highly advantageous. On the other hand, the use of ligands forms a common thread in most analytical methods developed for iron detection and in turn total organic ligand quantifications in seawater. The high degree of specificity of these ligands contributes directly to the low LOD that were achieved. In this way, the thermodynamic binding coefficients are of critical importance.

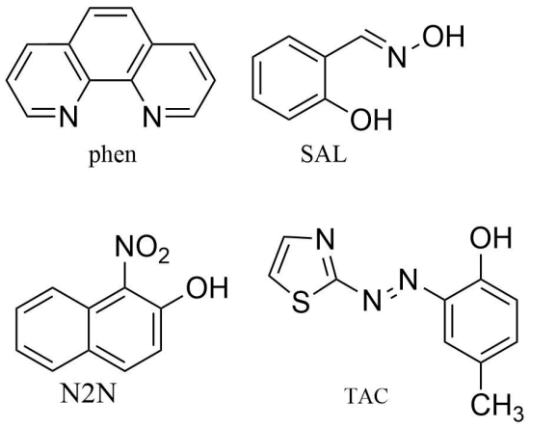

Figure 2.1: Ligand structures with associated abbreviations including 1,10-phenanthroline (phen), salicylaldoxime (SAL), 1-nitroso-2-naphthol (N2N), and 2-(2-thiazolylazo)-*p*-cresol (TAC).

Herein, our goal was to evaluate the electrochemical liquid|liquid interface as a potential alternative platform to HDME and modified surface electrode methods for total iron determination

as well as to investigate the overall binding strength of commonly used ligands. Electrochemistry at an immiscible interface between two electrolyte solutions (ITIES) offers the advantage of a molecularly smooth interface that is very reproducible without the need for extensive polishing or surface characterization;[17] in this way, it mimics the HDME interface without Hg's toxicity. Current at the liquid|liquid interface between water|oil (w|o) is measured *via* charge transfer across the ITIES through multiple routes; however, the three most common are simple and ligand assisted (facilitated) ion transfer as well as electron transfer reactions.[17a] To detect total iron in an aqueous sample four ligands were evaluated as depicted in Figure 2.1 against $FeSO_4$ dissolved in the aqueous phase towards an electrolytically controlled facilitated ion transfer (FIT) mechanism. The FIT reaction can be described for a generic ligand (*L*) *via* equation 1,

$$\mathrm{Fe}_w^{2+} + nL_o \rightleftharpoons \left[\mathrm{Fe}\text{-}L\right]_{n,o}^{2+} \qquad (2.1)$$

Overall complexation constants (β) and Fe^{2+}:ligand stoichiometric ratios (1:*n*) were determined through established thermodynamics developed from first principles by Girault's group;[18] Kakiuchi and Senda;[19] and Samec *et al*.[20] To enhance the sensitivity of the electrochemical measurements, a micro-ITIES (25 μm in diameter) positioned at the end of a pulled borosilicate glass pipette was used; the aqueous phase was installed inside the pipette and immersed in a 1,2-dichloroethane (DCE) solution containing the ligand and supporting electrolyte. The micro-ITIES is advantageous as it virtually eliminates *i*R drop owing to the low currents employed and the ITIES can be easily refreshed for high-throughput sampling.[21]

Thermodynamic constants discovered here differed somewhat relative to those previously reported. This is likely owing to the use of the w|DCE interface, where earlier data was based on

the w|Hg one, as well as a large excess of ligand employed herein, whereas, previous *apparent* complexation constant results relied on very small (μM) ligand concentration levels.

2.5 Results and Discussion

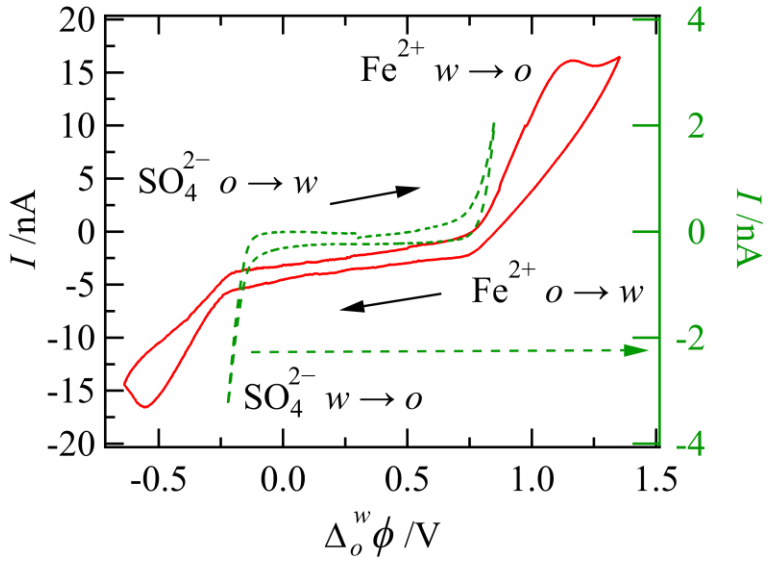

Figure 2.2: Cyclic voltammograms (CVs) recorded using Cell 2.1 with no ligand added to the DCE phase and with a scan rate of 0.020 V s^{-1}. The green, dashed curve shows the CV obtained when the polarizable potential window (PPW) is stopped at the conventional limit, while the red, solid trace describes the response when the potential scan exceeds this limit and Fe^{2+} and SO_4^{2-} ion transfer is observed as indicated inset.

The potential across the ITIES is controlled by an electrode immersed in either phase with the potential drop (or Galvani potential difference) localized across a few nanometers of the interface;[22] $\phi_w - \phi_o = \Delta_o^w\phi$. Blank cyclic voltammograms (CVs) employing Cell 2.1 with no ligand added to the organic phase have been plotted in Figure 2.2. The green trace (right axis) shows the typical CV obtained with the positive and negative potential ends of the polarizable

potential window (PPW) limited by the transfer of supporting electrolyte in the aqueous phase;[23] in this case, Fe^{2+} from water to oil ($w \rightarrow o$) at the positive potential limit and SO_4^{2-} from $w \rightarrow o$ at the negative potential end. While electroosmotically induced movement of micro and nano-ITIES has been observed at the tip of pipettes[24] and exploited for small volume electroosmotic sampling,[25] this movement can be eliminated by controlling the volume within the pipette *via* a syringe attached to the modified pipette holder.[23b, 23c, 26] This has been previously demonstrated by Ding's group.[23b, 23c] Thus, potentials beyond the conventional PPW can be explored at standard supporting electrolyte concentrations. In this way, the red, solid curve (left axis) in Figure 2.2 was obtained with the two peak-shaped waves, one at 1.194 V and the other at –0.554 V, corresponding to the simple ion transfer of Fe^{2+} and SO_4^{2-} from $w \rightarrow o$ with half-wave potentials $\left(\Delta_o^w \phi_{1/2}\right)$ of 1.180 and –0.540 V, respectively. Owing to the asymmetric diffusion regime at the micropipette tip,[21, 27] when an ion is transferred from $w \rightarrow o$ or from $o \rightarrow w$ across the ITIES a peak or sigmoidal shaped wave is recorded owing to the linear diffusion regime inside the pipette and hemispherical/radial one outside,[28] respectively. These data are in good agreement with previous reports of simple ion transfer at micro-ITIES held at the tip of glass pipettes.[21, 23b, 23c, 28]

Next, the system was tested with the four ligands (see Figure 2.1) by varying their concentrations individually from 20-60 mM in the case of phen, TAC, and SAL, and from 50-250 mM for N2N in the DCE phase. Upon addition of phen, N2N, or SAL in Cell 2.1 a peak shaped wave was observed (Figure 2.3A) with $\Delta_o^w \phi_{1/2}$ of 0.240, 0.867, and 0.971 V, respectively, with L = 50 mM. For N2N (Figure 2.3B) and SAL (Figure 2.3C), the peaks were not well defined and so the peak potentials used to determine $\Delta_o^w \phi_{1/2}$ were estimated based on changes in the slope of the curve as it approached the limit of the PPW. The $\Delta_o^w \phi_{1/2}$ shifted towards more negative

potentials concomitantly with increasing [L] (see Figure B1 Appendix B). These peaks were recognized as the facilitated ion transfer of Fe^{2+} by phen, N2N, or SAL and agree well with previous reports of ligand assisted transfer at liquid|liquid interfaces.[27, 29] The shift in the facilitated half-wave potential $\left(\Delta_o^w\phi_{1/2,ML_n^{z+}}\right)$ is in good agreement with established thermodynamics of facilitated ion transfer developed by Samec *et al.*;[20] Sendai and Kakiuchi;[19] as well as Girault's group.[18] Moreover, while experimenting with L = phen in Cell 2.1, a red solution was observed to form in the vicinity of the ITIES during electrochemically induced facilitated ion transfer. This colouration is likely due to the formation of $Fe(phen)_3^{2+}$ (*i.e.*, ferroin) complex, which is often employed in the Belousov-Zhabotinsky oscillating reaction;[13b, 30] ferroin is red when the iron core is in the 2+ oxidation state.

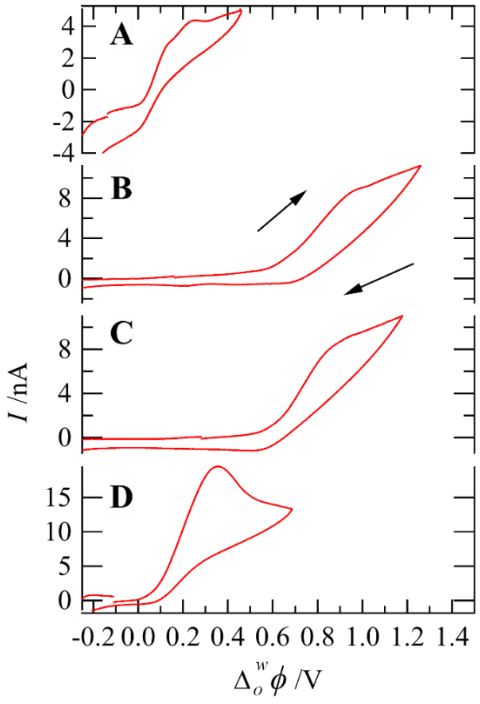

Figure 2.3: CVs generated using Cell 2.1 with 5 mM of $FeSO_4$ in the aqueous phase and *L* = phen (**A**), N2N (**B**), and SAL (**C**), as well as Cell 2.2 with 5 mM of HCl (*aq*) and *L* = phen (**D**). In each case, [*L*] = 50 mM and $v = 0.020$ V s^{-1}.

The complexation of phen with protons was also evaluated using Cell 2.2 with 5 mM HCl (*aq*) and [*L*] = 50 mM in the organic phase; the resultant CV has been graphed in panel D of Figure 2.3. By comparison of the $\Delta_o^w\phi_{1/2,ML_n^{z+}}$, a semi-quantitative trend in ligand binding can be developed such that, from strongest to weakest they are, Fe^{2+}-phen > H^+-phen > Fe^{2+}-N2N $\approx$ Fe^{2+}-SAL. Addition of TAC to Cell 2.1 resulted in a highly resistive CV (see Figure B2 of Appendix B) as evidenced by the large potential difference between the onset and peak potential for SO_4^{2-} transfer (~1.07 V); therefore, facilitated ion transfer by TAC was not investigated by CV.

Using the fundamentally derived thermodynamic solution relating the bulk/initial ligand concentration $\left(c_L^*\right)$ with the change in $\Delta_o^w\phi_{1/2,ML_n^{z+}}$ developed by Reymond *et al.*,[18] the ligand stoichiometry (*n*) and overall complexation constant (β) can be determined *via* the following,

$$-\frac{zF}{RT}\left(\Delta_o^w\phi_{1/2,ML_n^{z+}} - \Delta_o^w\phi_{M^{z+}}^{o'}\right) = n\ln\left(c_L^*\right) + \ln\left(\beta\right) \qquad (2.2)$$

where z, F, R, and T have their usual thermodynamic meaning. For CV measurements, $\Delta_o^w\phi_{Fe^{2+}}^{o'}$ = 1.18 V determined above was employed, while for proton coordination $\Delta_o^w\phi_{H^+}^{o'}$ = 0.58 V[23a] was used. For simplicity, it is assumed that the ligands are sufficiently hydrophobic so that their partitioning into the aqueous phase is negligible. Therefore, the mechanism shown in equation 1 is followed such that facilitated ion transfer proceeds either by transfer through interfacial

complexation (TIC) or ion transfer followed by organic phase complexation (TOC). TIC and TOC mechanisms are indistinguishable thermodynamically by this method.[18]

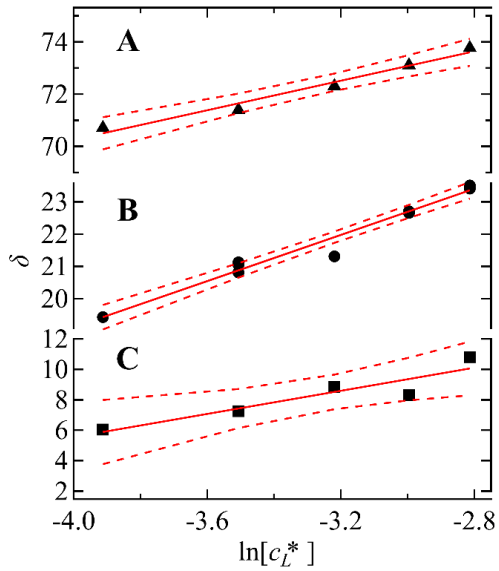

Figure 2.4: plots of $\delta = -zF/RT\left(\Delta_o^w\phi_{ML_n^{z+},1/2} - \Delta_o^w\phi_{M^{z+}}^{o'}\right)$ versus $\ln\left[c_L^*\right]$ for Cell 2.1 with L = phen (▲, **A**) and SAL (●, **B**), as well as for Cell 2.2 with L = phen (■, **C**) and 5 mM of HCl in the aqueous phase. The associated solid, red traces are the linear regression fittings while the red, dashed curves were obtained from the standard deviation of the linear fittings using a 95% confidence interval as described by Skoog *et al.*[31]

The linear trends of $-zF/RT\left(\Delta_o^w\phi_{ML_n^{z+},1/2} - \Delta_o^w\phi_{M^{z+}}^{o'}\right)$ versus $\ln\left[c_L^*\right]$ from equation 2 have been plotted in Figure 2.4 (markers) for the following ion-ligand combinations: Fe^{2+}-phen (A), Fe^{2+}-SAL (B), and H^+-phen (C). Linear regression fittings (solid lines) and the standard deviation with respect to the linear regression analysis (dashed curves) using a 95% confidence interval as described in Skoog *et al.*[31] and recently[32] are also plotted in Figure 2.4. A definitive trend for

the Fe^{2+} complexation with N2N and TAC could not be established through CV and were instead analyzed using differential pulse voltammetry (DPV) as described below. The Fe^{2+}-phen system resulted in 3 peaks on the forward CV scan (Figure 2.3A); however, individual peaks could not be resolved so an averaged peak position was utilized. The linear regression analysis shown graphically in Figure 2.4 and summarized in Table 2.1, resulted in R^2 values of 0.972 and 0.979 for Fe^{2+}-phen and Fe^{2+}-SAL complexation, respectively, demonstrating an excellent linear trend, while H^+-phen experiments lead to an R^2 of 0.855. Based on these analyses, metal ion:ligand stoichiometries (1:*n*) of roughly 1:3, 1:3, and 1:4 for Fe^{2+}-phen, Fe^{2+}-SAL and H^+-phen with β values of 2.7×10^{35}, 3.2×10^{14} and 8.8×10^{8}, respectively, were determined. The large difference between the β values of Fe^{2+} and H^+ is owing to their large differences in formal ion transfer potentials.

Table 2.1 Summary of linear regression data from Figure 2.4.

M	***L***	***n***	**ln(β)**	**R^2**
Fe^{2+}	phen	2.8	81.5	0.974
	SAL	3.6	33.4	0.972
H^+	phen	3.8	20.6	0.855

The CV shown in Figure 2.2 (red, solid trace) becomes resistive and capacitive after simple Fe^{2+} transfer is induced when the PPW is scanned beyond its normal limits; this is also true for most of the CVs in which Fe^{2+}-ligand assisted transfer is taking place. The increased

resistance/capacitance may be owing to the depletion of ions inside the microchannel at the pipette tip; see Figure B3 of the Appendix for an optical image of the pipette tip. The increased resistance/capacitance may artificially inflate the value of $\Delta_o^w\phi_{Fe^{2+}}^{o'}$ as well as the value of $\Delta_o^w\phi_{1/2,ML_n^{z+}}$ and the resultant overall complexation constant. Therefore, DPV was also performed to mitigate these effects. DPV has been a vital pulse protocol for resolving simultaneous electrochemical responses[23b, 23c, 29a, 33] as well as overcoming background current effects. From the DPV shown in Figure 2.5A, $\Delta_o^w\phi_{Fe^{2+}}^{o'}$ was determined using the potential at peak maximum $\left(\Delta_o^w\phi_{max}\right)$ and the following relationship,[34]

$$\Delta_o^w\phi_{max} = \Delta_o^w\phi^{o'} + \frac{RT}{zF}\ln\sqrt{\frac{D_w}{D_o}} - \frac{\Delta E}{2} \qquad (2.3)$$

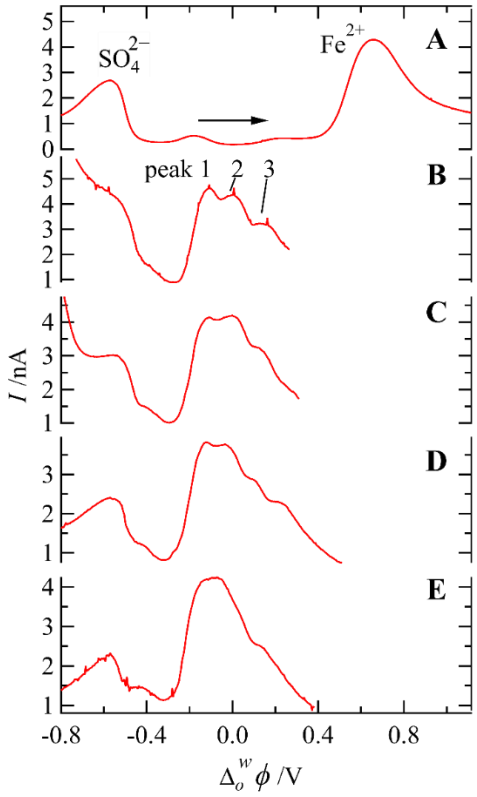

Figure 2.5: Differential pulse voltammograms (DPVs) recorded using Cell 2.1 with *L* = phen and [*L*] varied from 0-60 mM (A-E). The blank curve (A) was obtained without any ligand added to the organic phase. A pulse amplitude, width, and period of 50 mV, 50 ms, and 0.5 s were employed throughout.

Where ΔE is the pulse amplitude, while D_w and D_o are the ions diffusion coefficients in either phase. It was assumed that $D_w = D_o$; thus, the central term is removed. In this way, $\Delta_o^w\phi^{o'}_{Fe^{2+}}$ was calculated to be ~0.66 V, which is in good agreement with other hydrophilic multivalent metal ions such as strontium ($\Delta_o^w\phi^{o'}_{Sr^{2+}}$ = 0.654 V), dioxouranium ($\Delta_o^w\phi^{o'}_{UO_2^{2+}}$ = 0.699 V),[23c] and magnesium ($\Delta_o^w\phi^{o'}_{Mg^{2+}}$ = 0.644 V).[35] The formal ion transfer potential of H^+ was also determined using this method (see Appendix B, Figure B4) providing $\Delta_o^w\phi^{o'}_{H^+}$ = 0.584 V; this is in excellent agreement with $\Delta_o^w\phi^{o'}_{H^+}$ values reported by Olaya *et al*.[23a] (0.580 V) and Zhou *et al*.[35] (0.579 V).

Moving forward, Cell 2.1 with *L* = phen, N2N, TAC, and SAL was analyzed using DPV. When 20 mM of phen was added to Cell 2.1 (Figure 2.5B), three peaks could be resolved at –0.109, –0.001, and 0.139 V. These peaks moved to more negative potentials with increasing ligand concentration and represent the facilitated ion transfer of Fe^{2+} by phen from *w* to *o*. At [phen] = 40 mM a fourth peak seems to emerge towards higher potentials; however, it was not present at any other concentration and was therefore not analyzed. At high [phen], the peaks merge and become difficult to distinguish (Figure 2.5E); in this case, multi-peak fitting was used to identify $\Delta_o^w\phi_{max}$. Admittedly, multi-peak fitting is not ideal and comprehensive simulation that takes into account the diffusion of species in both phases would be preferable; however, the development of a complex simulation is beyond the scope of this work. Figure 2.6 shows the DPV responses when

N2N, TAC, or SAL is added to Cell 2.1 (see also Figures B4 and B5 of Appendix B); only one facilitated ion transfer peak could be discerned in each case. In the case of TAC and SAL the peak widths for facilitated Fe^{2+} were broad and may indicate the presence of multiple stoichiometries and coordination pathways; however, as a first approximation only one stoichiometry was analyzed. All four ligand systems were analyzed using equation 2.2 along with equation 2.3 to determine $\Delta_o^w\phi_{1/2,ML_n^{z+}}$ through the peak current at $\Delta_o^w\phi_{\max}$. Figure 2.7 shows the trends in $\Delta_o^w\phi_{1/2,ML_n^{z+}}$ with changing ligand concentration for the three peaks associated with phen (A-C), as well as singular SAL and N2N peak according to equation 2.2. To elicit a significant potential change so as to be observable, larger concentrations of N2N versus the other ligands studied was required; the linear trend for N2N has been plotted in Figure B6 (see Appendix B). Similar to the CV experiments above, each trend was analyzed using linear regression analysis with the results summarized in Table 2.2.

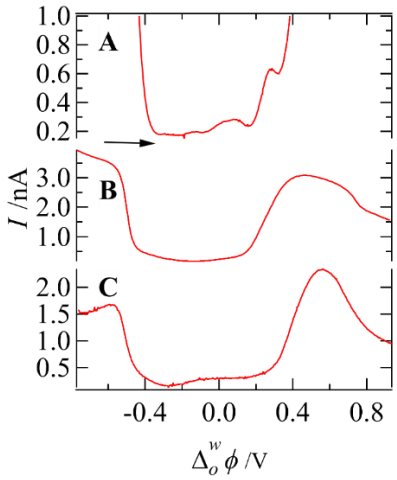

Figure 2.6: DPVs obtained using Cell 2.1 with *L* = N2N, TAC, and SAL at 150, 50, and 50 mM, respectively. All other instrument parameters were the same as described in Figure 2.5.

For phen, peaks 1, 2, and 3 had slopes of 1.5, 5.4, and 3.3 which indicates the metal ion:ligand stoichiometries of roughly 1:2, 1:5, and 1:3 with overall complexation constants of 5.6×10^{27}, 3.8×10^{30}, and 3.5×10^{22}, respectively. The R^2 values are representative of good linear fitting (see Table 2).

Ferroin or Fe^{2+}-$phen_3$ (*i.e.*, $n = 3$) is a well-known, widely used iron complex with highly reversible electrochemistry. β for $n = 3$ is in good agreement with that determined by Brisbin and McBryde[36] with magnitudes of 10^{23} for modified phenanthroline molecules, 5,6-dimethylphenanthroline and 4,7-dimethylphenathroline. Moreover, this result is in fair agreement with that determined by McKenzie[37] and more recently by Shalaby and Mohamed[38] of 2×10^{21} for the tris-1,10-phenanthroline-iron complex itself. The latter result is not a direct measurement of the complexation constant, but an effective one; moreover, both research groups performed their experiments at μM ligand concentrations, while here they were at mM levels. These two factors likely contribute to the difference between the two values. The 1:5 stoichiometry is likely the result of the relatively high [*L*] employed in Cell 2.1 relative to $[Fe^{2+}]$. The 1:2 stoichiometry is seemingly incongruent with its position relative to the other peaks potential and may be the result of partial protonation of the complex increasing/decreasing the overall charge of the complex while simultaneously influencing its hydration sphere. Additionally, peak 1 may be the result of multiple irons tethered together $[Fe_m^{2+}(phen)_n]$ and crossing the interface. If one assumes $m = 2$ and the total charge of the complex is 4+, then $n = 3$ and $\beta = 10^{55}$. Admittedly, this complexation constant is high and while the exact mechanism behind this complexation peak is unclear, it will be confirmed through future spectroelectrochemical experiments that are beyond the scope of the present work.

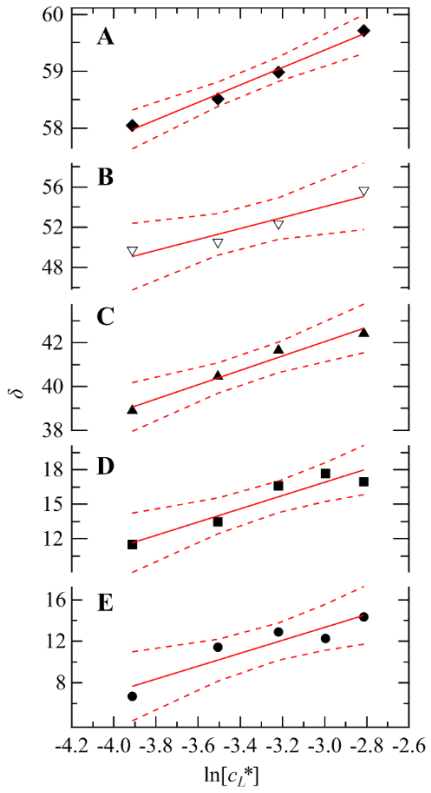

Figure 2.7: $\delta = -zF/RT\left(\Delta_o^w\phi_{ML_n^{z+},1/2} - \Delta_o^w\phi_{M^{z+}}^{o'}\right)$, with $\Delta_o^w\phi_{ML_n^{z+},1/2}$ taken from the experimental DPV curves shown in Figures 5 and 6, versus $\ln\left[c_L^*\right]$; whereas, L = phen (**A** (peak 3), **B** (peak 2), and **C** (peak 1)), TAC (**D**), and SAL (**E**).

Table 2.2 Linear regression data tabulated from Figures 7, S5, and S6 (see ESI).

M	***L***	***n***	**ln(*β*)**	**R^2**
Fe^{2+}	phen (peak 1)	1.5	63.9	0.988
	phen (peak 2)	5.4	70.4	0.921
	phen (peak 3)	3.3	51.9	0.974
	N2N	2.4	37.2	0.916
	TAC	5.8	34.2	0.901
	SAL	6.2	32.0	0.864

Values for n = 1 and 2 for SAL have been previously evaluated by Abualhaija *et al*.,[10q] which were indirectly determined using cathodic stripping voltammetry and referred to as *complex stability* constants; these were reported as $\log K_{n=1}$ = 6.50 and $\log \beta_{n=2}$ = 10.85, which equate to overall complexation constants of 3.2×10^6 and 7.1×10^{10}. The high n = 6 value for SAL determined here is owing to the high ligand concentrations employed and results in an overall complexation constant of 7.9×10^{13}. While this is 3 orders of magnitude higher than that reported by Abualhaija *et al*. for n = 2, it likely means that the 4 additional SAL molecules associated with Fe^{2+} reported here are only weakly bound. Sterically, this should be possible; however, each SAL molecule

would likely only bind once through either the lone-pair of electrons on the nitrogen or either hydroxyl group forming an octahedral geometry around the Fe core.

Similarly, complexation constants for Fe^{2+}(TAC) and $Fe^{2+}(TAC)_2$ of 1×10^{8} and 3.2×10^{17}, respectively, were reported by Croot *et al*.[10b] for a water/dioxane mixture; however, the β value for $Fe^{2+}(TAC)_6$ listed in Table 2 is 7.1×10^{14} for a water|DCE interface. As reported previously, complexation constants can differ between solvent systems. For example, during our previous study[29d] at the water|ionic liquid and w|DCE interfaces two β values were determined for the strontium octyl-(phenyl)-N,N-diisobutylcarbamoyl-methylphosphine oxide (CMPO) complex for $Sr^{2+}(CMPO)_3$ of 5.5×10^{25} and 1.5×10^{34}, respectively, which agreed with ionic liquids ability to capture metal ions in a facilitated ion transfer mechanism more effectively. Therefore, it is possible that some of the discrepancies seen here may be owing to the use of different solvent systems. Indeed, most complexation constants are reported for a HDME in an aqueous solution[5, 10a, 10b, 10d-r] which may be influenced by the water|Hg liquid interface.

2.6 Conclusion

Herein, 4 ligands common to electrochemical and spectroscopic detection of iron in seawater have been investigated using a w|DCE micro-ITIES installed at the tip of a pulled pipette. The objective was to determine the overall binding strength of Fe^{2+} as a model iron species to each of the ligands using established thermodynamics for facilitated ion transfer at a liquid|liquid interface.[18] $FeSO_4$ salt was dissolved in MilliQ, ultrapure water as both analyte and supporting electrolyte to avoid any interference from other metal ions. However, in future work simulated sea

and estuary water as well as other environmental samples will be tested to determine the effectiveness of this method as a practical, portable system for iron detection.

Similar to the standard redox potential at a solid electrode, the formal ion transfer for Fe^{2+} at the w|DCE interface was determined to be 0.660 V using DPV and scanning beyond the conventional PPW. Using this value, overall complexation constants for $Fe^{2+}(N2N)_2$, $Fe^{2+}(TAC)_6$, and $Fe^{2+}(SAL)_6$ were determined to be 1.4×10^{16}, 7.1×10^{14}, and 7.9×10^{13}, respectively, which are in fair agreement with other β constants determined indirectly by cathodic stripping voltammetry. With respect to phen complexation, three peaks were elucidated with peak 2 and 3 providing complex stoichiometries of $Fe^{2+}(phen)_5$ and $Fe^{2+}(phen)_3$ with $\beta = 3.8\times10^{30}$ and 3.5×10^{22}, respectively. The latter result is in good agreement with spectroscopic determinations.[6b, 37-38] Peak 1 provided an $n = 1$ and $\ln\beta = 63.9$, which was incongruous with its potential of facilitated ion transfer. This will be the focus of future tandem spectro-electrochemical investigations; however, it was speculated that it could represent a pseudo-polymeric form of the complex, *i.e.*, $[Fe_m(phen)_n)^{2m+}]$. DPV was necessary to eliminate the high capacitative current developed by this system, which may be owing to the low diffusion coefficient of Fe^{2+} or depletion of ions within the microchannel of the pulled pipette.

These data are an invaluable step forward towards implementing the electrolytic liquid|liquid interface as a platform for iron characterization in environmental water samples. Additionally, the thermodynamic parameters should be useful for Fe-ligand studies.

2.7 Experimental Section

All chemicals were used as received without further purification, unless indicated otherwise. Lithium sulfate monohydrate ($Li_2SO_4 \cdot H_2O$, ≥99%), iron (II) sulfate heptahydrate ($FeSO_4 \cdot 7H_2O$, ≥99%), salicylaldoxime (SAL, ≥98%), 1-nitroso-2-naphthol (N2N, 97%), 2-(2-thiazolylazo)-*p*-cresol (TAC, 97%), 1,10-phenanthroline monohydrate (≥99%), 1,2-dichloroethane (DCE, ≥99%), dichloromethane (>99%), hydrochloric acid (ACS reagent, 37%), 1-bromooctane (99%), and trioctylphosphine (97%) were obtained from Sigma-Aldrich. Tetrakis(pentafluorophenyl)borate lithium etherate ($Li(Et_2O)_nTB$, >99%) was purchased from Boulder Scientific (Boulder, CO). All aqueous solutions were prepared in MilliQ filtered ultrapure water (≥18.2 MΩ cm).

The organic phase supporting electrolyte tetraoctylphosphonium tetrakis(pentafluorophenyl)borate ($P_{8888}TB$) was prepared by first reacting equimolar amounts of 1-bromooctane with trioctylphosphine in a pressure tube (ACE glass) under nitrogen overnight with heating (~60°C); a clear ionic liquid tetraoctylphosphonium bromide ($P_{8888}Br$) was obtained and combined in equimolar amounts with $Li(Et_2O)_nTB$ in dichloromethane in air and allowed to stir overnight. The dichloromethane phase was washed 5 times with ~100 mL of MilliQ water, collected, and removed under vacuum. A white solid was obtained (m.p. ~53°C) and confirmed *via* NMR as has been detailed elsewhere.[26-27, 29b, 39]

All electrochemical experiments were performed using a CH Instruments potentiostat (Model#CHI602E) incorporating a liquid|liquid interface, or interface between two immiscible electrolytic solutions (ITIES), positioned at the tip of a micropipette held inside a modified pipette holder with integrated working electrode; the holder and pipette preparation have been detailed elsewhere.[26-27] The diameter of the ITIES was 25 μm as confirmed optically (see Figure B3 of

Appendix B). Two electrolytic cells were employed with the working electrode lead connected to a Pt wire integrated into the modified pipette holder and with the counter/reference electrode lead attached to a second Pt wire immersed in the organic phase.

$$\mathrm{Pt}\left|\mathrm{PtSO_4}\right|\underset{(aq)}{5\text{ mM }\mathrm{FeSO_4}}\Big\|\underset{(DCE)}{\substack{Y\text{ mM }L\\5\text{ mM }\mathrm{P_{8888}TB}}}\Big|\mathrm{PtTB}\Big|\mathrm{Pt} \qquad \text{[Cell 2.1]}$$

$$\mathrm{Pt}\left|\mathrm{PtCl_2}\right|\underset{(aq)}{5\text{ mM HCl}}\Big\|\underset{(DCE)}{\substack{Y\text{ mM }L\\5\text{ mM }\mathrm{P_{8888}TB}}}\Big|\mathrm{PtTB}\Big|\mathrm{Pt} \qquad \text{[Cell 2.2]}$$

Here, Y mM's of ligand (L) with L = phen, SAL, TAC, or N2N were added to the DCE phase; the double vertical line indicates the polarizable ITIES. All potentials were referenced to the simple, formal ion transfer potential of SO_4^{2-} ($\Delta_o^w\phi^{o'}_{SO_4^{2-}}$ = –0.540 V)[35] unless otherwise indicated.

2.8 References

[1] R. F. Strzepek, P. W. Boyd, W. G. Sunda, *Proc. Natl. Acad. Sci. U. S. A.* **2019**, *116*, 4388-4393.

[2] C. B. Field, M. J. Behrenfeld, J. T. Randerson, P. Falkowski, *Science* **1998**, *281*, 237.

[3] B. S. Twining, S. B. Baines, *Ann. Rev. Mar. Sci.* **2013**, *5*, 191-215.

[4] P. J. Worsfold, M. C. Lohan, S. J. Ussher, A. R. Bowie, *Mar. Chem.* **2014**, *166*, 25-35.

[5] (a) H. Obata, C. M. G. van den Berg, *Anal. Chem.* **2001**, *73*, 2522-2528; (b) C. M. G. van den Berg, *Anal. Chem.* **2006**, *78*, 156-163.

[6] (a) B. L. Lewis, P. D. Holt, S. W. Taylor, S. W. Wilhelm, C. G. Trick, A. Butler, G. W. Luther, *Mar. Chem.* **1995**, *50*, 179-188; (b) M. Lin, X. Hu, D. Pan, H. Han, *Talanta* **2018**, *188*, 135-144.

[7] (a) K. W. Bruland, R. P. Franks, G. A. Knauer, J. H. Martin, *Anal. Chim. Acta* **1979**, *105*, 233-245; (b) W. M. Landing, K. W. Bruland, *Geochim. Cosmochim. Acta* **1987**, *51*, 29-43.

[8] F. A. J. Armstrong, *J. Mar. Biol. Assoc. U. K.* **1957**, *36*, 509-517.

[9] (a) D. W. King, H. A. Lounsbury, F. J. Millero, *Environ. Sci. Technol.* **1995**, *29*, 818-824; (b) D. W. O'Sullivan, A. K. Hanson, D. R. Kester, *Mar. Chem.* **1995**, *49*, 65-77.

[10] (a) C. Sukekava, J. Downes, H. A. Slagter, L. J. A. Gerringa, L. M. Laglera, *Talanta* **2018**, *189*, 359-364; (b) P. L. Croot, M. Johansson, *Electroanalysis* **2000**, *12*, 565-576; (c) L. D. Nguyen, T. S. Vinh Nguyen, T. M. Huynh, R. Baptist, T. Chanh Duc Doan, C. M. Dang, *Electrochim. Acta* **2019**, *320*, 134607; (d) L. M. Laglera, D. Monticelli, *Curr. Opin. Electrochem.* **2017**, *3*, 123-129; (e) C. S. Hassler, F.-E. Legiret, E. C. V. Butler, *Mar. Chem.* **2013**, *149*, 63-73; (f) J. Wu, G. W. Luther, *Mar. Chem.* **1995**, *50*, 159-177; (g) E. L. Rue, K. W. Bruland, *Mar. Chem.* **1995**, *50*, 117-138; (h) M. Gledhill, C. M. G. van den Berg, *Mar. Chem.* **1995**, *50*, 51-61; (i) M. Gledhill, C. M. G. van den Berg, *Mar. Chem.* **1994**, *47*, 41-54; (j) K. Yokoi, C. M. G. van den Berg, *Electroanalysis* **1992**, *4*, 65-69; (k) C. M. G. van den Berg, M. Nimmo, O. Abollino, E. Mentasti, *Electroanalysis* **1991**, *3*, 477-484; (l) C. M. G. van den Berg, Z. Q. Huang, *J. Electroanal. Chem. Interfacial Electrochem.* **1984**, *177*, 269-280; (m) M. D. Granado-Castro, M. J. Casanueva-Marenco, M. D. Galindo-Riaño, H. El Mai, M. Díaz-de-Alba, *Mar. Chem.* **2018**, *198*, 56-63; (n) C. Genovese, M. Grotti, J. Pittaluga, F. Ardini, J. Janssens, K. Wuttig, S. Moreau, D. Lannuzel, *Mar. Chem.* **2018**, *203*, 28-37; (o) M. Lin, D. Pan, X. Hu, F. Li, H. Han, *Anal. Methods* **2015**, *7*, 5169-5174; (p) S. Caprara, L. M. Laglera, D. Monticelli, *Anal. Chem.* **2015**, *87*, 6357-6363; (q)

M. M. Abualhaija, C. M. G. van den Berg, *Mar. Chem.* **2014**, *164*, 60-74; (r) C. M. G. van den Berg, *Mar. Chem.* **1995**, *50*, 139-157.

[11] R. J. M. Hudson, D. T. Covault, F. M. M. Morel, *Mar. Chem.* **1992**, *38*, 209-235.

[12] (a) A. V. Korshunov, B. Yosypchuk, M. Heyrovsky, *Collect. Czech. Chem. Commun.* **2011**, *76*, 929-936; (b) D. V. Vukomanovic, D. E. Zoutman, G. S. Marks, J. F. Brien, G. W. van Loon, K. Nakatsu, *J. Pharmacol. Toxicol. Methods* **1996**, *36*, 97-102.

[13] (a) A. Bobrowski, J. Zarębski, *Electroanalysis* **2000**, *12*, 1177-1186; (b) T. J. Stockmann, J.-M. Noël, S. Ristori, C. Combellas, A. Abou-Hassan, F. Rossi, F. Kanoufi, *Anal. Chem.* **2015**, *87*, 9621–9630.

[14] (a) M. Ewert, J. W. Deming, *Biology* **2013**, *2*, 603-628; (b) K. Meiners, C. Krembs, R. Gradinger, *Aquat. Microb. Ecol.* **2008**, *52*, 195-207.

[15] J. P. Pinheiro, R. Domingos, R. Lopez, R. Brayner, F. Fiévet, K. Wilkinson, *Colloids and Surfaces A: Physicochemical and Engineering Aspects* **2007**, *295*, 200-208.

[16] B. Liu, M. Wang, *J. New Mater. Electrochem. Syst.* **2014**, *17*, 1-4.

[17] (a) M. D. Scanlon, E. Smirnov, T. J. Stockmann, P. Peljo, *Chem. Rev.* **2018**, *118*, 3722-3751; (b) P. Peljo, H. H. Girault, in *Encyclopedia of Analytical Chemistry*, John Wiley & Sons, Ltd, **2012**.

[18] F. Reymond, G. Lagger, P.-A. Carrupt, H. H. Girault, *J. Electroanal. Chem.* **1998**, *451*, 59-76.

[19] T. Kakiuchi, M. Senda, *J. Electroanal. Chem.* **1991**, *300*, 431-445.

[20] Z. Samec, D. Homolka, V. Mareček, *J. Electroanal. Chem. Interfacial Electrochem.* **1982**, *135*, 265-283.

[21] S. Liu, Q. Li, Y. Shao, *Chem. Soc. Rev.* **2011**, *40*, 2236-2253.

[22] C. Wei, A. J. Bard, M. V. Mirkin, *J. Phys. Chem.* **1995**, *99*, 16033-16042.

[23](a) A. J. Olaya, M. A. Méndez, F. Cortes-Salazar, H. H. Girault, *J. Electroanal. Chem.* **2010**, *644*, 60-66; (b) T. J. Stockmann, A.-M. Montgomery, Z. Ding, *J. Electroanal. Chem.* **2012**, *684*, 6-12; (c) T. J. Stockmann, A.-M. Montgomery, Z. Ding, *Can. J. Chem.* **2012**, *90*, 836-842.

[24] S. E. C. Dale, P. R. Unwin, *Electrochem. Commun.* **2008**, *10*, 723-726.

[25] (a) B. P. Nadappuram, P. Cadinu, A. Barik, A. J. Ainscough, M. J. Devine, M. Kang, J. Gonzalez-Garcia, J. T. Kittler, K. R. Willison, R. Vilar, P. Actis, B. Wojciak-Stothard, S.-H. Oh, A. P. Ivanov, J. B. Edel, *Nat. Nanotechnol.* **2019**, *14*, 80-88; (b) C. C. Chau, S. E. Radford, E. W. Hewitt, P. Actis, *Nano Lett.* **2020**, *20*, 5553-5561.

[26] T. J. Stockmann, R. Guterman, P. J. Ragogna, Z. Ding, *Langmuir* **2016**, *32*, 12966–12974.

[27] T. J. Stockmann, J.-M. Noel, A. Abou-Hassan, C. Combellas, F. Kanoufi, *J. Phys. Chem. C* **2016**, *120*, 11977–11983.

[28] A. Molina, E. Laborda, R. G. Compton, *Chem. Phys. Lett.* **2014**, *597*, 126-133.

[29] (a) E. D. Burgoyne, T. J. Stockmann, A. F. Molina-Osorio, R. Shanahan, G. P. McGlacken, M. D. Scanlon, *J. Phys. Chem. C* **2019**, *123*, 24643-24650; (b) T. J. Stockmann, L. Angelé, V. Brasiliense, C. Combellas, F. Kanoufi, *Angew. Chem. Int. Ed.* **2017**, *56*, 13493-13497; (c) T. J. Stockmann, A.-M. Montgomery, Z. Ding, *Anal. Chem.* **2012**, *84*, 6143-6149; (d) T. J. Stockmann,

Y. Lu, J. Zhang, H. H. Girault, Z. Ding, *Chem. Eur. J.* **2011**, *17*, 13206-13216; (e) T. J. Stockmann, Z. Ding, *Anal. Chem.* **2011**, *83*, 7542-7549; (f) F. Reymond, P.-A. Carrupt, H. H. Girault, *J. Electroanal. Chem.* **1998**, *449*, 49-65; (g) N. Nishi, H. Murakami, S. Imakura, T. Kakiuchi, *Anal. Chem.* **2006**, *78*, 5805-5812; (h) J. Langmaier, Z. Samec, *Anal. Chem.* **2009**, *81*, 6382-6389; (i) N. T. Iwai, M. Kramaric, D. Crabbe, Y. Wei, R. Chen, M. Shen, *Anal. Chem.* **2018**, *90*, 3067-3072.

[30] (a) R. Tomasi, J.-M. Noel, A. Zenati, S. Ristori, F. Rossi, V. Cabuil, F. Kanoufi, A. Abou-Hassan, *Chem. Sci.* **2014**, *5*, 1854-1859; (b) T. Arimura, M. Mukai, *Chem. Commun.* **2014**, *50*, 5861-5863; (c) J. Delgado, N. Li, M. Leda, H. O. Gonzalez-Ochoa, S. Fraden, I. R. Epstein, *Soft Matter* **2011**, *7*, 3155-3167.

[31] D. A. Skoog, F. J. Holler, S. Crouch, *Principles of Instrumental Analysis*, 6th ed., Thomson Higher Education, Belmont, CA, **2007**.

[32] E. D. Burgoyne, A. F. Molina-Osorio, R. Moshrefi, R. Shanahan, G. P. McGlacken, T. J. Stockmann, M. D. Scanlon, *Analyst* **2020**, *145*, 7000-7008.

[33] (a) M. l. D. Scanlon, G. g. Herzog, D. W. M. Arrigan, *Anal. Chem.* **2008**, *80*, 5743-5749; (b) A. M. O'Mahony, M. D. Scanlon, A. Berduque, V. Beni, D. W. M. Arrigan, E. Faggi, A. Bencini, *Electrochem. Commun.* **2005**, *7*, 976-982.

[34] H. Girault, *Analytical and Physical Electrochemistry*, 1st ed., EPFL Press, Lausanne, CH, **2004**.

[35] M. Zhou, S. Gan, L. Zhong, X. Dong, J. Ulstrup, D. Han, L. Niu, *Phys. Chem. Chem. Phys.* **2012**, *14*, 3659-3668.

[36] D. A. Brisbin, W. A. E. McBryde, *Can. J. Chem.* **1963**, *41*, 1135-1141.

[37] H. McKenzie, *Aust. J. Chem.* **1955**, *8*, 569-570.

[38] A. A. Shalaby, A. A. Mohamed, *Chem. Papers* **2020**, *74*, 3589-3595.

[39] T. J. Stockmann, P. D. Boyle, Z. Ding, *Catal. Today* **2017**, *295*, 89-94.

Chapter 3

Fe^{2+} complexation reactions characterized electrochemically at a micro aqueous|ionic liquid interface

3.0 Co-authorship Statement

The chapter comprises preliminary work investigating the above titled research program: Q. Jiang and T.J. Stockmann (2021) *In-preparation*. Experimental design by TJS. Experiments performed and analyzed by QJ. First draft prepared by TJS. Edited by QJ and TJS; finalized by TJS.

3.1 Introduction

Phytoplankton are a key organism in carbon and nitrogen fixation as well as ocean ecology; [1] they often form the base of the food chain in the ocean and are essentially responsible for carbon transfer (*i.e.*, carbon dioxide, CO_2) from the atmosphere to marine sediments – the so-called 'biological carbon pump'.[2] Nitrogenase, the enzyme responsible for nitrogen fixation in diatoms, consists of an iron core which functions as the active site; indeed, iron is a common component of many enzymes related to cellular respiration and is thus an essential micronutrient that can limit phytoplankton growth in so-called 'High Nutrient - Low Chlorophyll' (HNLC) zones.[3] Therefore, the spatiotemporal monitoring of iron in coastal and seawaters as well as from terrestrial sources is of special interest. As described in Chapter 1 and section 2.4, a wide breath of analytical methods has been developed to detect iron in the sub-nanomolar range – typical iron concentrations in

seawater.[4] The majority of these methods employ a ligand to enhance the selectivity towards iron and limit interference from other metals. These features culminate in extremely low limits of detection that are required for this type of trace metal analysis. This means that ligand binding coefficients (*i.e.*, complexation constants) are critical; however, they are only ever measured indirectly by most analytical methods.[5]

Electrochemical methods have predominantly employed a hanging drop mercury electrode (HDME) in conjunction with iron specific ligands;[6] however, Hg-electrodes have several disadvantages such as poor interfacial stability and toxicity. In Chapter 2, as well as elsewhere,[7] we proposed the liquid|liquid interface as an alternative electroanalytical platform in which a direct measurement of the overall complexation constant (β) can be determined along with the overall stoichiometry (n) of the metal ion-complexation reaction (see equations 1.7 and 2.1 as well as Figure 1.4). Through this technique we were able to obtain both values of Fe^{2+} coordination to 4 ligands (see Figure 2.1) that have been used extensively in the field for >50 years at the water|1,2-dichloroethane (w|DCE) micro-interface.[7]

In this section, an aqueous|ionic liquid (w|IL) interface was employed towards voltammetric investigation of Fe^{2+} facilitated ion transfer reactions using the ligand 1,10-phenanthroline (phen). The interface was made immiscible through the use of a highly hydrophobic ionic liquid (IL), tetraoctylphosphonium tetrakis(pentafluorophenyl)borate ($P_{8888}TB$),[8] that has been previously used as a supporting electrolyte[8] as well as in other w|IL electrochemistry. $P_{8888}TB$ is highly symmetric, non-coordinating, and affords a wide liquid|liquid electrochemical polarizable potential window (PPW) of ~1.0 V. Using previously described analytical solutions for

liquid|liquid complexation reactions, an Fe^{2+}:phen binding ratio of 1:1 along with the overall complexation constant are determined.

3.2 Experimental

Chemicals were used as received without further purification unless indicated otherwise. Experimental details, including instrumentation and chemical sourcing are the same as described in section 2.7 except for the following points. In this investigation, an aqueous|ionic liquid (w|IL) micro-interface (25 μm in diameter) employing w|P_{8888}TB was generated at the tip of a pulled borosilicate glass pipette. Micro-pipette preparation has been described elsewhere[9] as well as in Appendix A. P_{8888}TB has a melting point of ~55°C;[8] therefore, to ensure that it was entirely liquid and to reduce its viscosity, the vial holder was maintained at 60°C using a hot-water circulator (Cole-Parmer, Polystat) with inlet/outlet taps integrated into the wall of the Faraday cage. Electrolytic cells shown below and similar to those described in section 2.7, were employed using the modified pipette holder with integrated working electrode.

$$\mathrm{Pt}\left|\mathrm{PtSO_4}\right|\begin{matrix}\text{2 mM TMACl}\\ \text{5 mM } \mathrm{FeSO_4}\\ (aq)\end{matrix}\Big\|\begin{matrix}Y\text{ mM phen}\\ (\mathrm{P_{8888}TB})\end{matrix}\Big|\mathrm{PtTB}\Big|\mathrm{Pt} \qquad \text{[Cell 3.1]}$$

$$\mathrm{Pt}\left|\mathrm{PtSO_4}\right|\begin{matrix}X\text{ mM } \mathrm{Na_2SO_4}\\ (aq)\end{matrix}\Big\|\mathrm{P_{8888}TB}\Big|\mathrm{PtTB}\Big|\mathrm{Pt} \qquad \text{[Cell 3.2]}$$

The micro-interface between the aqueous phase and the hydrophobic IL P_{8888}TB (tetraoctylphosphonium tetrakis(pentafluorophenyl)borate) was maintained at the tip of a pulled borosilicate glass pipette and is indicated by the double line in Cells 3.1 and 3.2 above (TB =

$B(C_6F_5)_4^-$). The concentration (*Y*) of the ligand 1,10-phenanthroline (phen) in Cell 3.1 was changed in the IL phase, while TMACl (tetramethylammonium chloride) was added to the aqueous phase for the purposes of referencing the potential; the formal ion transfer potential of TMA^+ $\left(\Delta_{IL}^{w}\phi_{TMA^+}^{o'}\right)$ was taken to be 0.270 V.[10] In Cell 3.2, the concentration (*X*) of Na_2SO_4 was changed from 5 to 400 mM to simulate electrolyte concentrations in seawater.

3.3 Results and Discussion

Figure 3.1A shows the *i*-V response using Cell 3.1 with no phen added to the IL phase (*i.e.*, *Y* = 0) nor TMACl added to the aqueous phase. The scan in the positive direction was initiated at –0.23 V and proceeded at a rate of 0.020 V s^{-1} until roughly 0.47 V, where it was then scanned in the reverse direction to –0.46 V. The sharp increase and decrease in current at the positive and negative ends of the voltammetric pulse are related to the simple ion transfer of the anionic ($B(C_6F_5)_4^-$, TB^-) and cationic (P_{8888}^+) components of the IL, respectively, as well as the supporting electrolyte ions in the aqueous phase;[11] thus, it describes the limits of the polarizable potential window (PPW). After addition of phen and TMACl to the IL and aqueous phases respectively (Figure 3.1B-E), two peak-shaped waves were observed at –0.127 and 0.337 V in the forward scan as well as at 0.205 and –0.192 V in the reverse one. The signal towards the positive end of the PPW is related to the simple ion transfer of TMA^+. [10, 12] The *i*-V profile in both forward and reverse directions is peak-shaped owing to two factors: (1) the asymmetric geometry of the micropipette tip and (2) the high viscosity of the IL phase. As described in section 2.5 and elsewhere,[13] the micro-ITIES geometry at a pipette tip results in hemispherical diffusion outside the capillary and linear diffusion regimes inside where the microchannel walls restrict mass

transport (see Figure B3 in Appendix B). This in turn results in a sigmoidal and peak-shaped *i*-V responses for ingress and egress of ions, respectively, across the ITIES.[13] However, owing to the high viscosity of the IL, mass transport and diffusion coefficients are greatly reduced in that phase; this transforms the usual hemispherical diffusion regime into a linear one in which simple ion transfer from IL→*w* elicits a peak-shaped voltammetric wave.[10, 14] These results agree well with previous reports.[8-9, 14-15] Therefore, the signal at roughly –0.2 V likely corresponds to facilitated ion transfer of Fe^{2+} by phen from *w*→IL during the forward sweep and from IL→*w* in the reverse scan; this can be summarized through equation 3.1 below,

$$Fe^{2+}(aq) + n\ phen(IL) \rightleftharpoons [Fe(phen)_n]^{2+}(IL) \qquad (3.1)$$

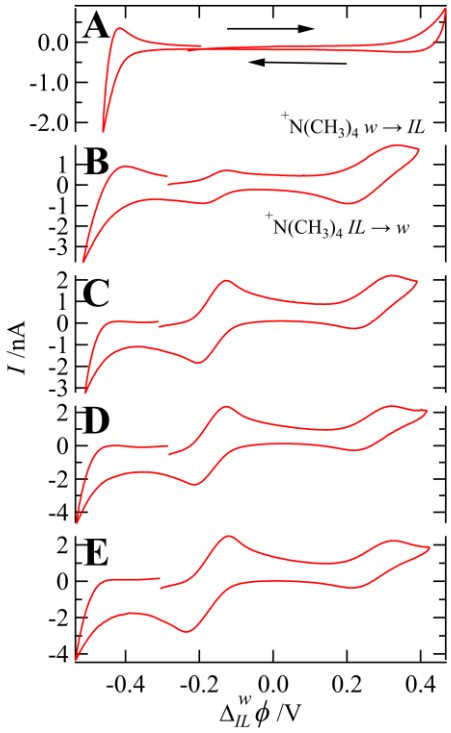

Fig. 3.1: The CV response obtained using Cell 3.1 at a scan rate of 0.020 V s^{-1} with increasing [phen] in the $P_{8888}TB$ phase from 0-60 mM (A-E). The simple ion transfer wave for $N(CH_3)_4^+$ has been labelled inset, while arrows indicate scan direction.

Equation 3.1 is similar to equation 2.1 encountered in Chapter 2. Increasing [phen] resulted in a concomitant decrease in the facilitated ion transfer half-wave potential $\left(\Delta_{IL}^{w}\phi_{ML_n^z,1/2}\right)$; *i.e.*, $\Delta_{IL}^{w}\phi_{ML_n^z,1/2}$ shifted to more negative potentials with increasing [phen]. For the w|IL interface, half-wave potentials were calculated as the mid-point between the peak maximums of the forward (*fwd*) and reverse (*rev*) waves or,

$$\Delta_{IL}^{w}\phi_{1/2} = \frac{\Delta_{IL}^{w}\phi_{\max,fwd} + \Delta_{IL}^{w}\phi_{\max,rev}}{2} \qquad (3.2)$$

If one assumes that phen is a neutral species and sufficiently hydrophobic such that it does not partition from *w*→IL, then facilitated Fe^{2+} transfer is entirely interfacial; thus, the 'transfer by interfacial complexation (TIC) mechanism' is preferred. The 3 dominant facilitated ion transfer mechanisms, including TIC, have been depicted in Figure 1.4. By assuming a TIC mechanism and having the bulk ligand concentration $\left(c_L^*\right)$ in excess of the aqueous metal ion concentration, then the analytical solution as proposed by Reymond *et al*.[16] is greatly simplified and similar to equation 2.2; however, owing to the high IL viscosity/low diffusion coefficients, a third term, $\ln\left(\xi\right)$, must be added such that one obtains,

$$-\frac{zF}{RT}\left(\Delta_{IL}^{w}\phi_{1/2,ML_n^{z+}} - \Delta_{IL}^{w}\phi_{M^{z+}}^{o'}\right) = n\ln\left(c_L^*\right) + \ln\left(\beta\right) + \ln\left(\xi\right) \qquad (3.3)$$

Where $\xi = \sqrt{D_{IL}/D_w}$ and D_{IL} and D_w are the diffusion coefficients of phen in the IL and aqueous phases, respectively, which are unknown; however, these were estimated to be 1×10^{-5} and 5×10^{-9} cm s^{-1}, respectively, which are based on the diffusion coefficient of ferrocene in $P_{8888}TB$ measured voltammetrically at an ultramicroelectrode.[12] This is admittedly a gross approximation and a question our group hopes to resolve before submitting this work for publication; we are presently exploring NMR spectroscopic as well as electrochemical methods for determining these two parameters. The ligand-free, simple ion transfer potential of Fe^{2+} $\left(\Delta_{IL}^{w}\phi_{Fe^{2+}}^{o'}\right)$ was estimated to be 0.55 V using the edge-of-scan profile from the blank CV and the working curve from ref [11d]. In this way, equation 3.3 is a linear trend with a slope of *n* and a *y*-intercept of $\left[\ln\left(\beta\right)+\ln\left(\xi\right)\right]$.

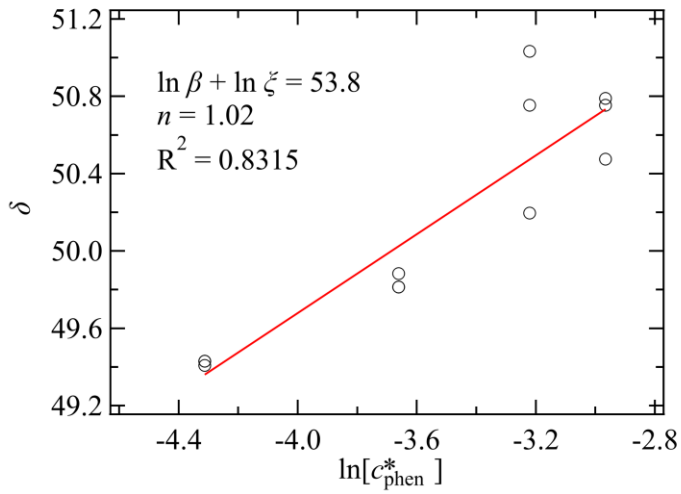

Fig. 3.2: Plot of $\delta = -\frac{zF}{RT}\left(\Delta_o^w\phi_{1/2,ML_n^z} - \Delta_o^w\phi_{M^{z+}}^{o'}\right)$ versus $\ln\left[c_{phen}^*\right]$ (○); where, c_{phen}^* was the initial, bulk concentration of phen in the $P_{8888}TB$ phase. Statistics from the linear regression analysis (red trace) are provided inset.

Using the above assumptions, the linear plot of $-\frac{zF}{RT}\left(\Delta_o^w\phi_{1/2,ML_n^z,} - \Delta_o^w\phi_{M^{z+}}^{o'}\right)$ versus $\ln\left[c_{phen}^*\right]$ shown in Figure 3.2 was developed. Linear regression analysis, red trace in Figure 3.2, revealed a slope of 1.02 and a *y*-intercept of 53.8 which translate to a Fe:phen stoichiometry of 1:1 and an overall complexation constant, β, equal to 1.04×10^{25}. β is related to the step wise complexation constants (K_n) *via*,

$$K_n = \frac{c_{ML_n^z,\alpha}}{c_{ML_{(n-1)}^z,\alpha}c_{L,\alpha}}, \text{ or, } \beta = \frac{c_{ML_n^z,\alpha}}{c_{M^z,\alpha}\left(c_{L,\alpha}\right)^n} = \prod_{k=0}^{n} K_{k,\alpha} \qquad (3.4)$$

Where the subscript α refers generally to the phase, either aqueous or IL. A proposed structure of the Fe(phen) complex is illustrated in Figure 3.3.

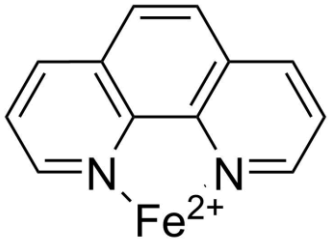

Figure 3.3: Proposed bidentate binding of phen to Fe^{2+}. Solvent molecules/hydration sphere have been neglected.

Comparing these values to those detailed in Chapter 2 for the two Fe: phen ratios observed at the w|DCE interface,[7] specifically 1:5 and 1:3 with $\beta = 3.8\times10^{30}$ and 3.5×10^{22}, respectively, one can see that even despite a lower metal to ligand ratio, the w|IL interface elicits higher binding coefficients. This agrees with the early metal extraction work performed by Dai *et al*.,[17] in which much higher extraction efficiencies were obtained for w|IL systems versus w|organic solvent ones.

The β value obtained herein is several orders of magnitude removed from that observed for Sr^{2+} coordination to CMPO[9a] ($n = 3$, $\beta = 1.5\times10^{34}$) at a w|P_{66614}TB micro-interface, as mentioned in the discussion section of section 2.5; however, this is likely due to the high ligand stoichiometry $[Sr(CMPO)_3]^{2+}$, relative to that observed here for Fe^{2+}, combined with the inherent binding strength. However, the overall complexation constant previously determined by Ding's group[9a] for the $[Sr(CMPO)_3]^{2+}$ was based on an estimated formal Sr^{2+} transfer potential of 1.033 V which was highly approximative. Indeed, Ding's group has studied a range of facilitated ion transfer processes using CMPO at w|IL micro-interfaces using both P_{8888}TB [8] and P_{66614}TB, [9a, 15] which were considered equivalent as a first approximation. K^+, Rb^+ and Cs^+ coordination to CMPO at these w|IL micro-interface were analyzed with the following complexes observed: $[K(CMPO)_3]^+$, $[K(CMPO)_2]^+$, $[Rb(CMPO)_2]^+$, and $[Cs(CMPO)_3]^+$ having β constants of 1×10^{13}, 8.9×10^6, 2.4×10^6,

and 1.6×10^{11}, respectively. In this way, the thermodynamic coefficients determined herein for $Fe(phen)^{2+}$ indicate a ligand/biphasic system that is highly coordinating.

The presence of a return peak upon scanning in the reverse direction indicates that the facilitated ion transfer process is likely reversible. In conventional electrochemistry at a large interface (mm scale) peak-to-peak separations are often employed to test the reversibility of an electron or ion transfer process; whereby, ~0.059/*z* V is the usual indicator that the process is reversible.[18] For IL systems however, peak-to-peak separations for ~0.100 V are common owing to the high viscosity, but do not necessarily mean the charge transfer process is irreversible.[12, 19] Therefore, it is likely that the facilitated ion transfer process observed here is reversible; however, further kinetic analysis is required to confirm this point.

Moving forward, Na_2SO_4 and NaCl are known to be salts at appreciable concentrations in seawater (e.g., [NaCl] ≈ 0.5 M), while at the same time, it is recognized that increasing the concentration of aqueous supporting electrolyte ions begins to limit the size of PPW.[11a-c, 20] Therefore, to investigate whether the w|IL interface could be employed directly towards the electroanalytical testing of seawater samples, Cell 3.2 was employed whereby the concentration of Na_2SO_4 was varied from 5 to 400 mM to see the influence on the PPW; Figure 3.4 shows the resultant differential pulse voltammograms (DPVs) obtained. At 5 and 400 mM Na_2SO_4 the PPW was roughly 1.0 and 0.35 V wide, respectively – an almost 70% reduction its size. Therefore, the number of phenomena that can be observed at seawater electrolyte concentrations is severely curtailed. This highlights a major limitation towards the direct application of liquid|liquid electrochemistry to seawater samples and likely indicates that analysis will have to be restricted to estuary environmental samples where the salt concentration is much lower.

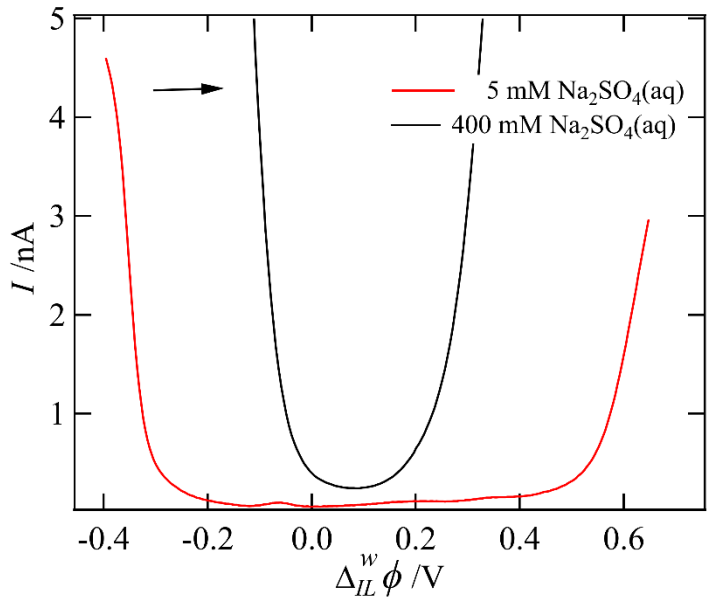

Figure 3.4: DPV obtained using Cell 3.1 with [Na_2SO_4] = 5 or 400 mM as indicated inset. All other instrument parameters were the same as described in Figure 2.5. The potential scale is the experimental one and has not been referenced to any ion transfer potential.

3.4 Conclusions

Herein, the w|IL micro-interface was employed to investigate the Fe^{2+} coordination reactions towards 1,10-phenanthroline. One Fe^{2+}: phen ligand stoichiometry was determined, Fe(phen) or n = 1, with an overall complexation constant of 1.04×10^{25}. These data suggest that the phen ligand, in combination with the w|P_{8888}TB interface, is highly coordinating towards Fe^{2+}, which agrees well with previous reports that show that $Fe(phen)_3^{2+}$ is a stable, highly reversible redox species often employed in electrochemical investigations.[21] Voltammetric waves indicate that the facilitated ion transfer process is likely reversible; however, further investigation is needed to explore the kinetics of this reaction. While environmental samples were not analyzed, these data

suggest the w|IL interface is promising for total iron quantification, likely in a method where ions are deposited at or in the vicinity of the interface through a sustained potentiostatic pulse and then 'stripped' off voltammetrically – similar to cathodic/anodic stripping voltammetry at a solid|solution interface.

These data are preliminary and more work at the w|IL interface, as well as the w|o one, is required to fully evaluate them as electroanalytical platforms for iron detection.

3.5 References

[1] R. F. Strzepek, P. W. Boyd, W. G. Sunda, *Proc. Natl. Acad. Sci. U. S. A.* **2019**, *116*, 4388-4393.

[2](a) S. Basu, K. R. M. Mackey, *Sustainability* **2018**, *10*, 869; (b) J. J. Pierella Karlusich, C. Bowler, H. Biswas, *Front. Plant Sci.* **2021**, *12*, 1-19.

[3] B. S. Twining, S. B. Baines, *Ann. Rev. Mar. Sci.* **2013**, *5*, 191-215.

[4] M. Lin, X. Hu, D. Pan, H. Han, *Talanta* **2018**, *188*, 135-144.

[5] M. Gledhill, L. J. A. Gerringa, *Frontiers in Marine Science* **2017**, *4*.

[6](a) L. M. Laglera, D. Monticelli, *Curr. Opin. Electrochem.* **2017**, *3*, 123-129; (b) H. Obata, C. M. G. van den Berg, *Anal. Chem.* **2001**, *73*, 2522-2528; (c) D. Jagner, L. Renman, S. H. Stefansdottir, *Anal. Chim. Acta* **1993**, *281*, 305-314; (d) C. M. G. van den Berg, M. Nimmo, O. Abollino, E. Mentasti, *Electroanalysis* **1991**, *3*, 477-484; (e) C. M. G. van den Berg, Z. Q. Huang, *J. Electroanal. Chem. Interfacial Electrochem.* **1984**, *177*, 269-280.

[7] Q. Jiang, H. E. Reader, T. J. Stockmann, *ChemElectroChem* **2021**, *8*, 1580-1587.

[8] T. J. Stockmann, P. D. Boyle, Z. Ding, *Catal. Today* **2017**, *295*, 89-94.

[9](a) T. J. Stockmann, Y. Lu, J. Zhang, H. H. Girault, Z. Ding, *Chem. Eur. J.* **2011**, *17*, 13206-13216; (b) T. J. Stockmann, Z. Ding, *Anal. Chem.* **2011**, *83*, 7542-7549.

[10] T. J. Stockmann, Z. Ding, *J. Phys. Chem. B* **2012**, *116*, 12826-12834.

[11] (a) A. J. Olaya, M. A. Méndez, F. Cortes-Salazar, H. H. Girault, *J. Electroanal. Chem.* **2010**, *644*, 60-66; (b) T. J. Stockmann, A.-M. Montgomery, Z. Ding, *J. Electroanal. Chem.* **2012**, *684*, 6-12; (c) T. J. Stockmann, A.-M. Montgomery, Z. Ding, *Can. J. Chem.* **2012**, *90*, 836-842; (d) T. J. Stockmann, Z. Ding, *Phys. Chem. Chem. Phys.* **2012**, *14*, 13949-13954.

[12] T. J. Stockmann, J. Zhang, J. C. Wren, Z. Ding, *Electrochim. Acta* **2012**, *62*, 8-18.

[13] (a) S. Liu, Q. Li, Y. Shao, *Chem. Soc. Rev.* **2011**, *40*, 2236-2253; (b) E. D. Burgoyne, A. F. Molina-Osorio, R. Moshrefi, R. Shanahan, G. P. McGlacken, T. J. Stockmann, M. D. Scanlon, *Analyst* **2020**, *145*, 7000-7008; (c) T. J. Stockmann, J.-M. Noel, A. Abou-Hassan, C. Combellas, F. Kanoufi, *J. Phys. Chem. C* **2016**, *120*, 11977–11983.

[14] N. Nishi, H. Murakami, S. Imakura, T. Kakiuchi, *Anal. Chem.* **2006**, *78*, 5805-5812.

[15] (a) T. J. Stockmann, J. Zhang, A.-M. Montgomery, Z. Ding, *Anal. Chim. Acta* **2014**, *821*, 41-47; (b) T. J. Stockmann, A.-M. Montgomery, Z. Ding, *Anal. Chem.* **2012**, *84*, 6143-6149.

[16] F. Reymond, G. Lagger, P.-A. Carrupt, H. H. Girault, *J. Electroanal. Chem.* **1998**, *451*, 59-76.

[17] S. Dai, Y. H. Ju, C. E. Barnes, *J. Chem. Soc., Dalton Trans.* **1999**, *8*, 1201-1202.

[18] A. J. Bard, L. R. Faulkner, *Electrochemical Methods: Fundamentals and Applications*, 2nd ed., John Wiley, New York, **2001**.

[19] (a) M. C. Buzzeo, O. V. Klymenko, J. D. Wadhawan, C. Hardacre, K. R. Seddon, R. G. Compton, *J. Phys. Chem. B* **2004**, *108*, 3947-3954; (b) J. E. F. Weaver, D. Breadner, F. Deng, B. Ramjee, P. J. Ragogna, R. W. Murray, *J. Phys. Chem. C* **2011**, *115*, 19379-19385.

[20] T. J. Stockmann, H. Deng, P. Peljo, K. Kontturi, M. Opallo, H. H. Girault, *J. Electroanal. Chem.* **2014**, *729*, 43-52.

[21] T. J. Stockmann, J.-M. Noël, S. Ristori, C. Combellas, A. Abou-Hassan, F. Rossi, F. Kanoufi, *Anal. Chem.* **2015**, *87*, 9621–9630.

Chapter 4

4.1 Conclusions and Perspectives

In Chapter 2, the w|DCE micro-ITIES was employed investigating four ligands common to other analytical methods of iron determination in seawater. Exploiting the analytical, thermodynamic solutions to facilitated ion transfer at liquid|liquid, immiscible interfaces previously developed by Reymond *et al.*,[1] the metal ion:ligand stoichiometry (1:*n*) and overall complexation constant (β) were determined for each ligand towards Fe^{2+} using cyclic and differential pulse voltammetries. For N2N, TAC, and SAL, the stoichiometries $Fe(N2N)_2^{2+}$, $Fe(TAC)_6^{2+}$, and $Fe(SAL)_6^{2+}$, where determined with β values of 1.4×10^{16}, 7.1×10^{14}, and 7.9×10^{13}, respectively. Surprisingly, using DPV, three Fe^{2+}-phen stoichiometries were resolved, including $Fe(phen)^{2+}$, $Fe(phen)_5^{2+}$, and $Fe(phen)_3^{2+}$, with respective β values of 5.6×10^{27}, 3.8×10^{30}, and 3.5×10^{22}. The magnitude of β for the $Fe(phen)^{2+}$ stoichiometry was incongruent with the location of the *i*-V response within the potential window leading to a mismatch in the magnitude of the $n = 1$ β value between the other two stoichiometries; however, more work needs to be done to elucidate this point, which may be possible using tandem spectroelectrochemical methods. Indeed, many iron-complexes, such as $Fe(phen)_3^{2+/3+}$ (ferroin),[2] absorb in the UV/Visible region (~510 nm)[3] generating a red/blue solution for the 2+/3+ oxidation states, respectively. The other stoichiometries agreed well with previous reports in the literature as described in sections 2.5 and 2.6. Additionally, the free metal ion transfer of Fe^{2+} $\left(\Delta_o^w\phi_{Fe^{2+}}^{o'}\right)$ at the w|DCE interface, a critical thermodynamic constant, was determined to be 0.660 V using DPV, which made the facilitated ion transfer analysis possible.

Meanwhile, in Chapter 3 preliminary results were presented towards the electroanalytical use of a water|ionic liquid (w|IL) micro-interface. Ionic liquids (ILs) are advantageous owing to their low vapour pressure as well as excellent thermal and electrochemical stability. Moreover, because they are composed of molecularly large organic cations and anions, one can modify their molecular architecture to achieve nearly an infinite array of them[4] so that one can fine tune their physciochemical properties such as hydrophobicity and viscosity. In this way, they are often considered to be 'designer solvents'.

In 1999 Dai *et al*. [5] published a seminal work in which they described an additional feature of ILs: a several orders of magnitude improvement in ligand assisted metal ion extraction efficiencies versus conventional molecular solvents. Thus, ILs could be another avenue to metal ion extraction selectivity. Herein, the IL tetraoctylphosphonium tetrakis(pentafluorophenyl)borate ($P_{8888}TB$) was employed as it has demonstrated excellent hydrophobicity and electrochemical stability [6] – important factors for building an electrochemical, liquid|liquid sensor. Similar to Chapter 2, phen mediated Fe^{2+} coordination reactions across a micro-interface between water|$P_{8888}TB$ were investigated, operating at 60°C. Only one stoichiometry was observed in this case, with $n = 1$ and $\beta = 1.04\times10^{25}$. While initial, these results are promising and point to a combination of ligand and IL that is highly sensitive; however, more work needs to be done to ensure selectivity versus other metal ions present in seawater.

Next, a model salt, Na_2SO_4, present at appreciable concentrations in seawater (~0.5 M), was used to investigate the influence that increased supporting electrolyte concentrations would have on the size of the PPW at the w|IL interface, since it is well known that the PPW for the w|o interface decreases concomitantly with aqueous electrolyte concentrations.[7] Unfortunately, a ~70%

decrease in the PPW was observed when increasing [Na_2SO_4] from 5 to 400 mM. This will present a unique challenge moving forward in the development of an Fe environmental sensor. However, several strategies are already being considered, including nanoparticle/IL functionalized electrodes such as that described recently by Li *et al*.;[8] whereby, reduced graphene-oxide (rGO) nanosheets, coated with an IL, were used to support gold nano-dendrite formations. Nano-functionalizing the interface enhances the electroactive surface area which can be combined with chemisorbed ligands in an IL microenvironment for enhanced analytical selectivity/sensitivity. Indeed, ligand functionalized nanoparticles (NPs) have been previously demonstrated by Liu *et al*. who employed Au NPs decorated with N-carboxy-L-cysteine as mentioned in section 2.4.[9] In this way, the electroanalytical methods employed herein can be used as a first step towards screening different ligand/IL combinations that then can be exploited for electrode modification.

The research program will continue to target less exotic, commercially available ligands; however, these can be expanded to include ones like EDTA (ethylenediamineethylacetic acid). According to Natsuike *et al*.'s work,[10] EDTA was successfully employed to investigate the kinetics of Fe uptake by micro-algae in terrestrial and coastal waters located in northeast Japan. The linear relationship between the concentration of Fe in water and the ratio of Fe utilized by algae indicated that the efficiency for algae absorbing Fe was controlled by the iron concentration, but the uptake ratio in river is much lower than in the ocean considering the same environmental iron concentration. Ferrozine (see Figure 4.1), which has been used extensively in the spectroscopic determination of dissolved Fe,[11] should also be targeted. Farid *et al*.[11a] recently demonstrated an improvement to the long-standing method for total dissolved iron and even tested it against competing ligands like EDTA.

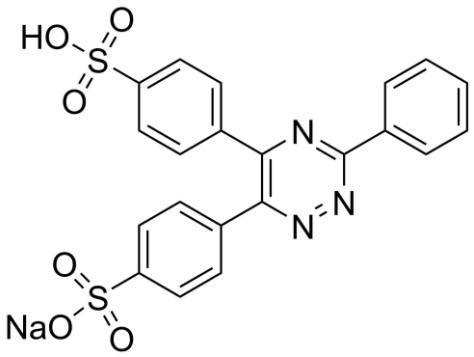

Figure 4.1: Chemical structure of ferrozine.

ILs incorporating a ligand moiety will be synthesized in our group, in this way, generating so-called task specific ionic liquids (TSILs). These will have the advantage of overcoming IL solubility issues that are common with neutral, non-ionized species,[12] thus limiting ligand loss/partitioning to the secondary phase. In the early 2000's, Roger's group [13] proposed a series of TSILs incorporating thiol and carbonyl moieties which are highly coordinating towards heavy metals like Cd^{2+} and Hg^{2+} as well as transuranic elements; a few examples of the IL cations have been drawn in Figure 4.2. This field has continued to expand and now includes anionic ligands, neutral ones like those described in these pages, as well as TSILs.[14]

The work described herein is an initial first step towards building a rich research program intersecting the fields of metal ion extraction as well as environmental sensors. While much more work needs to be done, the future is bright with possibilities.

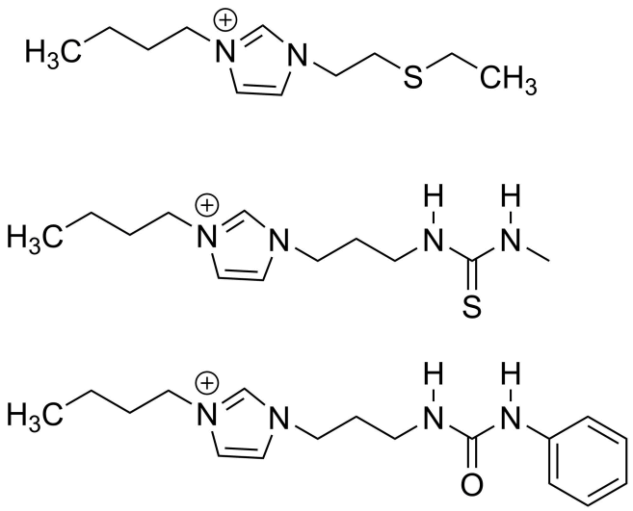

Figure 4.2: Structures of the cationic IL components paired with PF_6^- anions introduced by Visser *et al*.[13d]

4.2 References

[1] F. Reymond, G. Lagger, P.-A. Carrupt, H. H. Girault, *J. Electroanal. Chem.* **1998**, *451*, 59-76.

[2] T. J. Stockmann, J.-M. Noël, S. Ristori, C. Combellas, A. Abou-Hassan, F. Rossi, F. Kanoufi, *Anal. Chem.* **2015**, *87*, 9621–9630.

[3] E. C. Ellingsworth, B. Turner, G. Szulczewski, *RSC Adv.* **2013**, *3*, 3745-3754.

[4] (a) G. Adamova, R. L. Gardas, M. Nieuwenhuyzen, A. V. Puga, L. P. N. Rebelo, A. J. Robertson, K. R. Seddon, *Dalton Trans.* **2012**, *41*, 8316-8332; (b) G. Adamova, R. L. Gardas, L. P. N. Rebelo, A. J. Robertson, K. R. Seddon, *Dalton Trans.* **2011**, *40*, 12750-12764; (c) K. Dong, X. Liu, H. Dong, X. Zhang, S. Zhang, *Chem. Rev.* **2017**, *117*, 6636-6695.

[5] S. Dai, Y. H. Ju, C. E. Barnes, *J. Chem. Soc., Dalton Trans.* **1999**, 1201-1202.

[6] T. J. Stockmann, P. D. Boyle, Z. Ding, *Catal. Today* **2017**, *295*, 89-94.

[7] (a) T. J. Stockmann, H. Deng, P. Peljo, K. Kontturi, M. Opallo, H. H. Girault, *J. Electroanal. Chem.* **2014**, *729*, 43-52; (b) A. J. Olaya, M. A. Méndez, F. Cortes-Salazar, H. H. Girault, *J. Electroanal. Chem.* **2010**, *644*, 60-66.

[8] F. Li, D. Pan, M. Lin, H. Han, X. Hu, Q. Kang, *Electrochim. Acta* **2015**, *176*, 548-554.

[9] B. Liu, M. Wang, *J. New Mater. Electrochem. Syst.* **2014**, *17*, 1-4.

[10] M. Natsuike, Y. Endo, H. Ito, M. Miyamoto, C. Yoshimura, M. Fujii, *Estuar. Coast. Shelf Sci* **2020**, *235*, 106580.

[11] (a) H. Tohidi Farid, K. G. Schulz, A. L. Rose, *Mar. Chem.* **2018**, *203*, 22-27; (b) M. Lin, X. Hu, D. Pan, H. Han, *Talanta* **2018**, *188*, 135-144.

[12] (a) A. B. Pereiro, J. M. M. Araújo, F. S. Oliveira, J. M. S. S. Esperança, J. N. Canongia Lopes, I. M. Marrucho, L. P. N. Rebelo, *J. Chem. Thermodyn.* **2012**, *55*, 29-36; (b) T. J. Stockmann, J.-F. Lemineur, H. Liu, C. Cometto, M. Robert, C. Combellas, F. Kanoufi, *Electrochim. Acta* **2019**, *299*, 222-230.

[13] (a) A. E. Visser, M. P. Jensen, I. Laszak, K. L. Nash, G. R. Choppin, R. D. Rogers, *Inorg. Chem.* **2003**, *42*, 2197-2199; (b) A. E. Visser, R. P. Swatloski, W. M. Reichert, R. Mayton, S. Sheff, A. Wierzbicki, J. H. Davis, R. D. Rogers, *Environ. Sci. Technol.* **2002**, *36*, 2523-2529; (c) A. E. Visser, R. P. Swatloski, W. M. Reichert, R. Mayton, S. Sheff, A. Wierzbicki, J. J. H. Davis, R. D. Rogers, *Chem. Commun.* **2001**, 135-136; (d) A. E. Visser, J. D. Holbrey, R. D. Rogers, *Chem. Commun.* **2001**, 2484-2485.

[14] H. Okamura, N. Hirayama, *Anal. Sci.* **2021**, *37*, 119-130.

Appendix

A. Preparation of micro-capillary

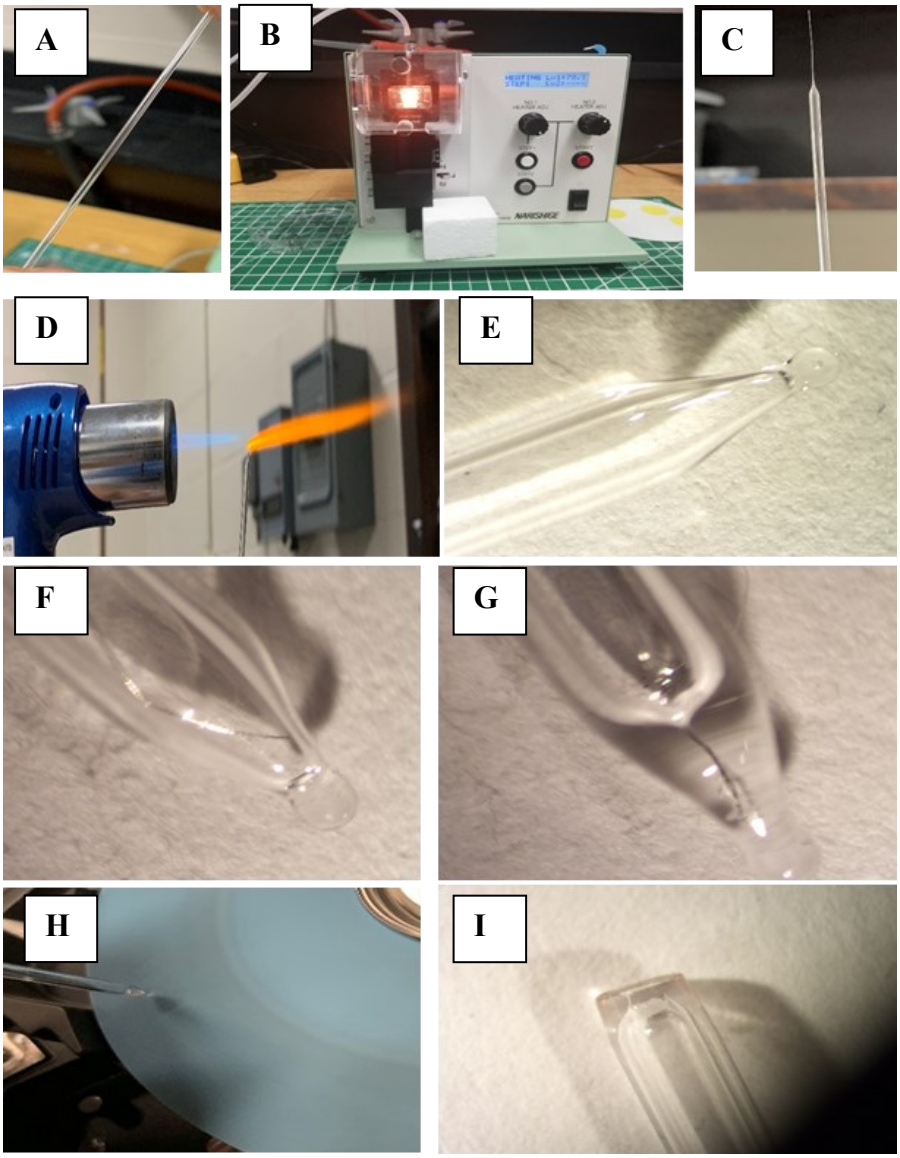

Figure A1: Steps of preparing a micro pipette. First, a borosilicate glass capillary (1.18 mm/2.00 mm inner/outer diameter, **A**, Goodfellow Inc.) was pulled with heating at its center

using an electric pipette puller (Narishige Inc., **B**) generating two tapered pipettes. The tapered ends (**C**) were flame sealed using a hand-torch (**D**) to create a ball of glass (**E**). Next a 25 μm-diameter Pt wire was inserted into the open end and pushed down the capillary using a copper wire until it was positioned inside the tapered end (**F**). Using the electric puller in a fixed position, the Pt wire was annealed in place (**G**). Next, the tapered end was polished using alumina polishing pads of increasingly finer grit (30-0.3 μm, Buehler) to expose the Pt wire cross-section and until the glass surface was smooth (**H**). Finally, the Pt wire was etched using aqua regia (3:1 HCl:HNO_3) for 48 hours to expose a microchannel with a diameter of 25 μm (**I**); see also Figure B3 in Appendix B.

B. Supporting Information for Chapter 2

B.1 Facilitated ion transfer CV responses for Fe^{2+}-phen, Fe^{2+}-SAL, and H+-phen

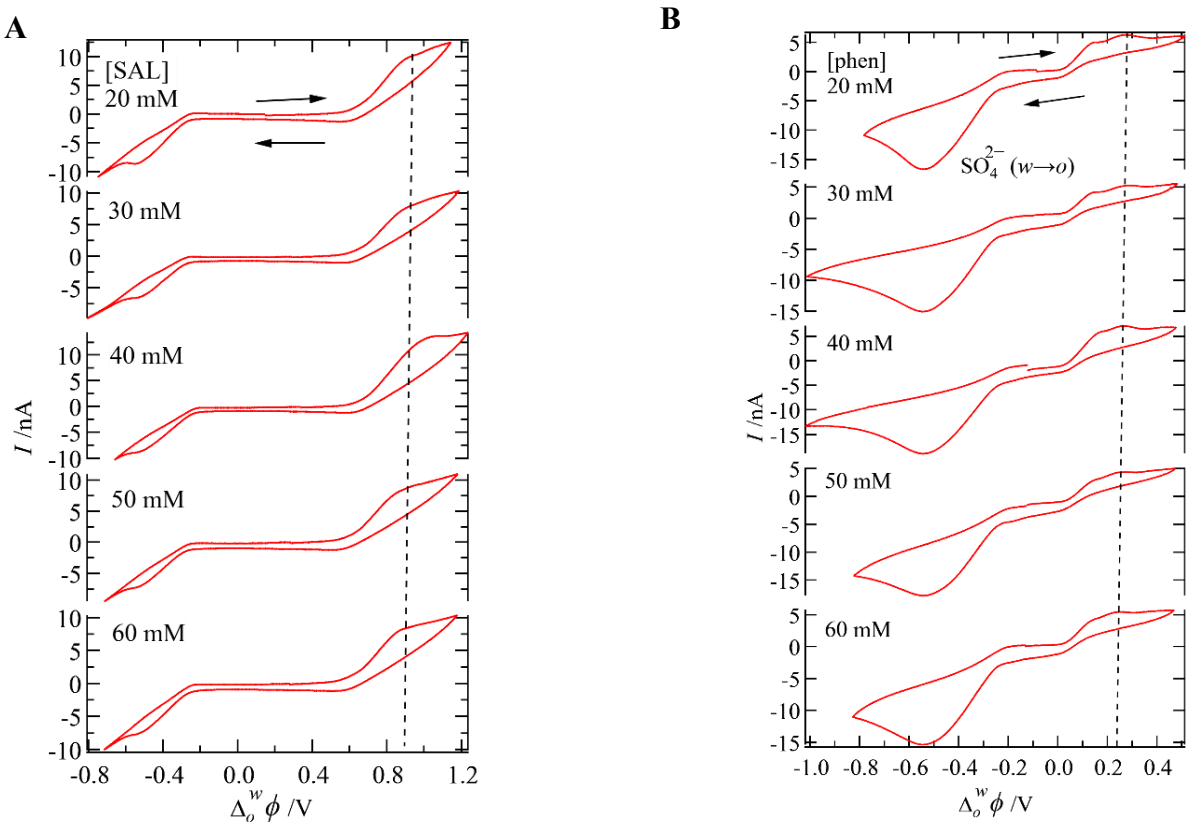

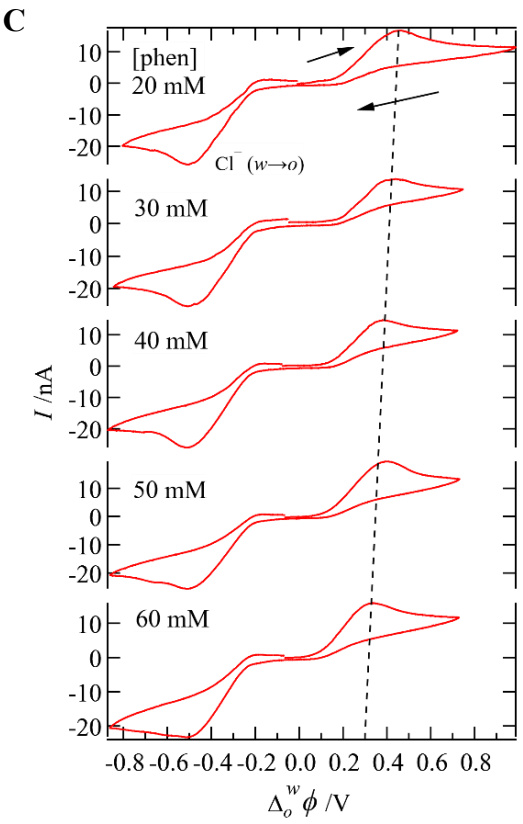

Figure B1: CVs obtained using Cell 2.1 with *L* = phen (A) and SAL (B) as well as Cell 2.2 with *L* = phen (C) whilst varying [*L*] as indicated inset. All other parameters were the same as those in Figure 2.2 in chapter 2. The dashed line indicates the general trend as peaks shift to lower potentials as [*L*] increases.

B.2 Cyclic voltammetric response for TAC facilitated Fe^{2+} transfer

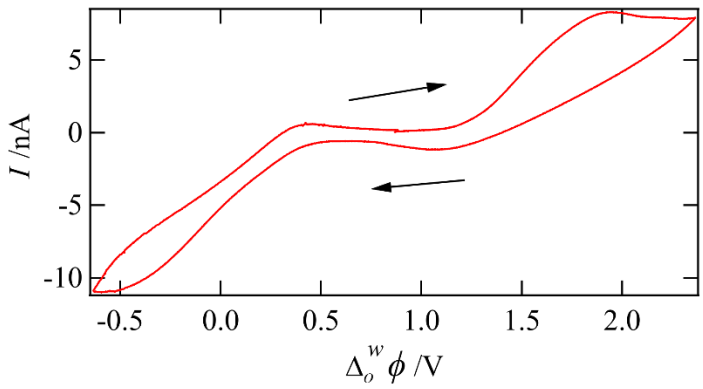

Figure B2: CV response recorded using Cell 2.1 with 40 mM of TAC in the DCE phase. All other parameters were the same as described in Figure 2.2 of Chapter 2.

B.3 Optical Image of the pipette tip

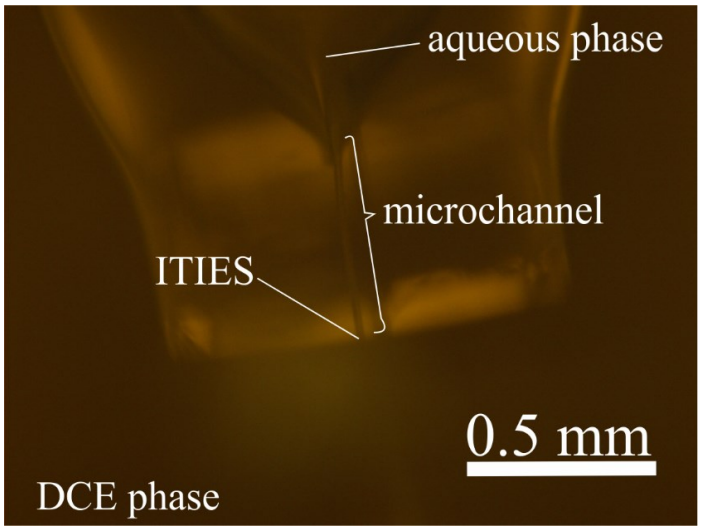

Figure B3: optical micrograph of the micropipette tip containing the aqueous phase and immersed in the DCE phase with the ITIES, or liquid|liquid interface (25 μm in diameter) held at the tip.

B.4 Differential Pulse Voltammetry of H^+ simple ion transfer

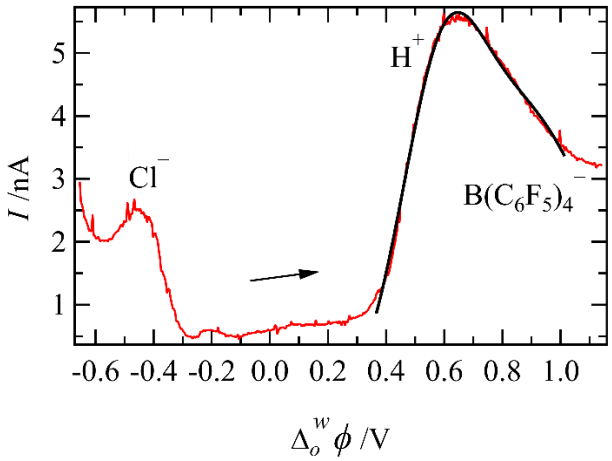

Figure B4: Differential Pulse Voltammogram of simple H^+ ion transfer using Cell 2.2 with no ligand added to the DCE phase (red trace). Instrument parameters were the same as those described in Figure 2.5 of chapter 2. Multi-peak curve fitting was performed to determine the peak location of the H^+ transfer (black trace).

B.5 Differential Pulse Voltammetry of facilitated Fe^{2+} transfer by SAL, TAC, and N2N

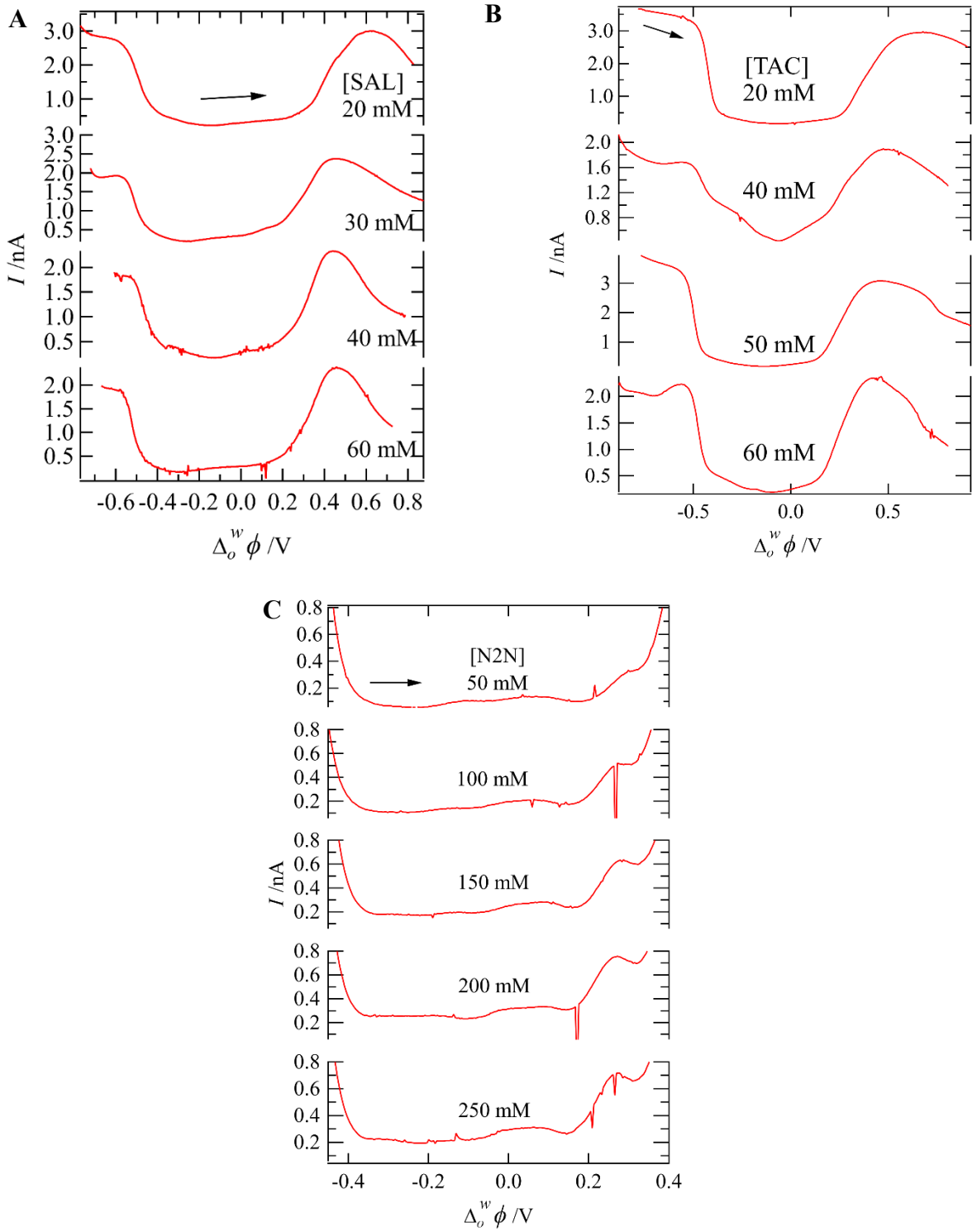

Figure B5: Plots of DPVs using Cell 2.1 with L = SAL (A), TAC (B) and N2N (C) with the concentrations changed as written inset. All other parameters were the same as indicated in Figure 2.5.

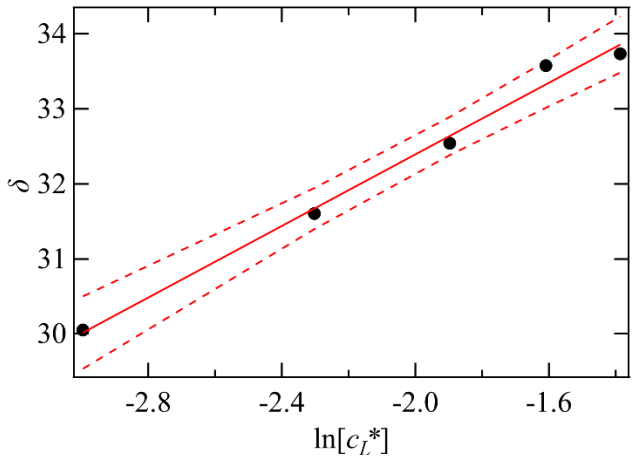

Figure B6: Trend of $\delta = -\frac{zF}{RT}(\Delta_o^w\phi_{ML_n^{z+},1/2} - \Delta_o^w\phi_{M^+}^{o'})$ versus $\ln[c_L^*]$ from equation 2.2 of the main text, where L = N2N, and $\Delta_o^w\phi_{ML_n^{z+},1/2}$ was obtained from DPVs depicted in Figure B5C.